Estimation of Depolarization Ratio Using Weather Radars with Simultaneous Transmission/Reception

ALEXANDER RYZHKOV,[a,b] SERGEY Y. MATROSOV,[c,d] VALERY MELNIKOV,[a,b] DUSAN ZRNIC,[b] PENGFEI ZHANG,[a,b] QING CAO,[e] MICHAEL KNIGHT,[e] CLEMENS SIMMER,[f] AND SILKE TROEMEL[f]

[a] *Cooperative Institute for Mesoscale Meteorological Studies, University of Oklahoma, Norman, Oklahoma*
[b] *NOAA/National Severe Storms Laboratory, Norman, Oklahoma*
[c] *Cooperative Institute for Research in Environmental Sciences, University of Colorado Boulder, Boulder, Colorado*
[d] *NOAA/Earth System Research Laboratory, Boulder, Colorado*
[e] *Enterprise Electronics Corporation, Enterprise, Alabama*
[f] *Meteorological Institute, University of Bonn, Bonn, Germany*

(Manuscript received 27 February 2016, in final form 25 March 2017)

ABSTRACT

A new methodology for estimating the depolarization ratio (DR) by dual-polarization radars with simultaneous transmission/reception of orthogonally polarized waves together with traditionally measured differential reflectivity Z_{DR}, correlation coefficient ρ_{hv}, and differential phase Φ_{DP} in a single mode of operation is suggested. This depolarization ratio can serve as a proxy for circular depolarization ratio measured by radars with circular polarization. The suggested methodology implies the use of a high-power phase shifter to control the system differential phase on transmission and a special signal processing to eliminate the detrimental impact of differential phase on the estimate of DR. The feasibility of the suggested approach has been demonstrated by retrieving DR from the standard polarimetric variables and the raw in-phase I and quadrature Q components of radar signals and by implementing the scheme on a C-band radar with simultaneous transmission/reception of horizontally and vertically polarized waves. Possible practical implications of using DR include the detection of hail and the determination of its size above the melting layer, the discrimination between various habits of ice aloft, and the possible identification and quantification of riming, which is associated with the presence of supercooled cloud water. Some examples of these applications are presented.

1. Introduction

Historically, the first dual-polarization weather radars transmitted radio waves with either linear or circular polarizations and received both the copolar and cross-polar components of the reflected signals. The ratio of powers of these components represents the depolarization ratio. By definition, the linear depolarization ratio L_{dr} is the ratio of the power of a cross-polar radar return to the power of a copolar radar return if a wave with horizontal (or vertical) polarization is transmitted (e.g., Bringi and Chandrasekar 2001). Circular depolarization ratio C_{dr} is the ratio of the power of the copolar component of the reflected signal (e.g., left-hand circular) to its cross-polar component (e.g., right-hand circular) (McCormick and Hendry 1975). Depolarization ratios are usually represented in a logarithmic scale [LDR = $10\log_{10}(L_{\mathrm{dr}})$ and CDR = $10\log_{10}(C_{\mathrm{dr}})$]. In previous studies, depolarization ratios have been used primarily for the identification of hail and the melting layer wherein both L_{dr} and C_{dr} are much higher than in pure rain and dry snow (e.g., Minervin and Shupyatsky 1963; Barge 1974; Bringi et al. 1986; Holler et al. 1994; Hubbert et al. 1998; Kennedy et al. 2001). It was also shown by Matrosov et al. (2001, 2012) that the CDR dependency on antenna elevation angle can be used to distinguish between planar and columnar types of ice cloud hydrometeors and to estimate the hydrometeor degree of nonsphericity (i.e., the deviation of their axis ratios from 1).

There are several important differences between LDR and CDR. First, CDR depends primarily on the

Corresponding author: Alexander Ryzhkov, alexander.ryzhkov@noaa.gov

DOI: 10.1175/JAMC-D-16-0098.1

scatterers' shape and only slightly on their orientations (in fact, CDR does not depend on the scatterer orientation in the incident wave propagation plane), whereas LDR depends both on the shape and (very strongly) on the orientation of hydrometeors. Second, CDR is generally larger than LDR (if the hydrometeors are nonspherical) and can be more reliably measured at low signal-to-noise ratio (SNR). For randomly oriented hydrometeors, CDR is 3 dB higher than LDR, and the difference between CDR and LDR increases for oriented nonspherical hydrometeors (Holt et al. 1999; Ryzhkov 2001). In rain, CDR can exceed LDR by more than 10 dB. On the negative side, CDR is much more sensitive to propagation effects than LDR. In other words, CDR strongly depends on differential phase Φ_{DP}; therefore, separating the contributions of backscattering and forward propagation effects to Φ_{DP} in interpreting CDR is a notoriously difficult task (e.g., Al-Jumily et al. 1991; Torlaschi and Holt 1993, 1998). This may limit the utilization of CDR close to the radar where Φ_{DP} is small.

Radar variables measured in linear and circular polarization bases are interrelated, and any single variable in a circular polarization basis, such as CDR, can be expressed via a combination of the variables measured in a linear horizontal–vertical (HV) polarization basis provided that all elements of the covariance scattering matrix in the HV basis are known along with the elements of the propagation matrix describing effects of differential attenuation and differential phase (e.g., Jameson 1987; Tragl 1990; Zrnić 1991; Krehbiel et al. 1996; Holt et al. 1999; Bringi and Chandrasekar 2001). Holt et al. (1999) attempted to estimate CDR using simultaneous and switched transmission of vertical and horizontal polarization implemented on the research CSU–CHILL polarimetric radar, which utilizes two transmitters and two receivers for orthogonal polarizations to obtain a full covariance scattering matrix (Brunkow et al. 2000).

Although circular polarized meteorological radars have been used in the past (e.g., McCormick and Hendry 1979; Kropfli et al. 1990; Krehbiel et al. 1996), modern operational dual-polarization radars increasingly use simultaneous transmission and reception of the waves of horizontal and vertical polarizations (SHV) with a single transmitter (Doviak et al. 2000), which allows measuring differential reflectivity Z_{DR}, differential phase Φ_{DP}, and copolar correlation coefficient ρ_{hv} but not LDR (in the SHV mode of operation). Some polarimetric weather radars optionally measure LDR in a special LDR mode of operation; then only a horizontally polarized wave is transmitted, and both the horizontally and vertically polarized radar returns are received. This mode of operation, however, requires a polarization switch on transmission, and simultaneous measurements of Z_{DR} and LDR are not possible. Most users do not utilize the LDR mode because switching back and forth between the SHV and LDR modes slows down the radar data update and causes premature wear of the high-power switch. Chandrasekar and Bharadwaj (2009) suggested a technique to estimate LDR in the SHV mode using phase coding. According to this technique, the horizontally and vertically polarized transmit waveforms are coded with orthogonal phase sequences. This phase coding is not implemented on operational polarimetric weather radars, and such an opportunity has been explored only on the research CSU–CHILL radar.

How much information do we lose by abandoning depolarization measurements, or is it still possible to infer depolarization characteristics of atmospheric particles in the standard SHV mode of operations? Matrosov (2004) was the first to propose the idea of measuring a proxy for the circular depolarization ratio by an X-band radar operating in the SHV mode. This idea was echoed in more recent investigations by Melnikov and Matrosov (2013) and Ryzhkov et al. (2014). In this study, we further explore such an approach and demonstrate how CDR—or its proxy, depolarization ratio (DR)—can be estimated from operational dual-polarization weather radar observations and thus complement Z_{DR}, Φ_{DP}, and ρ_{hv} data without slowing down or compromising the standard mode of operation. Moreover, we show that our method automatically eliminates the impact of propagation differential phase on DR (and thus CDR) estimates at the signal processor level. The best results are achieved if the system differential phase on transmission $\Phi_{DP}^{(t)}$ is controlled using a high-power phase shifter to ensure that the polarization state of the transmitted wave is close to circular.

2. Theoretical background

Typical signal processors of polarimetric radars estimate the powers of the received signals in the orthogonal channels P_h and P_v and the complex covariance R_{hv} from which the radar reflectivity, the differential reflectivity, the magnitude of correlation coefficient, and its phase (i.e., differential phase) are computed. If V_h and V_v are complex voltages of radar returns at the output of the two receivers for backscattered waves with horizontal and vertical polarizations, then

$$P_h = \overline{|V_h|^2}, \quad P_v = \overline{|V_v|^2}, \quad \text{and} \quad R_{hv} = \overline{V_h^* V_v}, \qquad (1)$$

where overbars indicate averaging over a number of radar samples, and the superscript * denotes the complex conjugate. In the SHV mode of operation whereby the horizontal (h) and vertical (v) waves are transmitted and received simultaneously, the complex voltages V_h and V_v are expressed as (Doviak et al. 2000; Matrosov 2004; Ryzhkov and Zrnić 2007)

$$\begin{pmatrix} V_h \\ V_v \end{pmatrix} = C' \begin{bmatrix} \exp j\Phi_{\mathrm{DP}}^{(r)} & 0 \\ 0 & 1 \end{bmatrix} \begin{pmatrix} T_h & 0 \\ 0 & T_v \end{pmatrix} \begin{pmatrix} S_{hh} & S_{hv} \\ S_{hv} & S_{vv} \end{pmatrix} \times \begin{pmatrix} T_h & 0 \\ 0 & T_v \end{pmatrix} \begin{bmatrix} \exp j\Phi_{\mathrm{DP}}^{(t)} \\ 1 \end{bmatrix}, \qquad (2)$$

where S_{ij} are the elements of the scattering matrix of hydrometeors in the horizontal–vertical linear polarization basis, T_i are the elements of the propagation matrix accounting for signal attenuation and propagation differential phase Φ_{DP}, and $\Phi_{\mathrm{DP}}^{(t)}$ and $\Phi_{\mathrm{DP}}^{(r)}$ are the system differential phases on transmission and reception, respectively. A zero-mean canting angle of the hydrometeors along a propagation path is assumed so that the transmission matrix $\mathbf{T}$ has a diagonal form. The propagation terms are ensemble averaged along the propagation path as opposed to the elements of the scattering matrix $\mathbf{S}$, which are ensemble averaged in the radar resolution volume. According to Eq. (2), the voltages in the two orthogonal channels are

$$V_h = C''\langle S_{hh} A_{hv} \exp\{j[-\Phi_{\mathrm{DP}} + \Phi_{\mathrm{DP}}^{(t)} + \Phi_{\mathrm{DP}}^{(r)}]\} + S_{hv} A_{hv}^{1/2} \exp\{j[-\Phi_{\mathrm{DP}}/2 + \Phi_{\mathrm{DP}}^{(r)}]\}\rangle \quad \text{and} \qquad (3)$$

$$V_v = C''\langle S_{hv} A_{hv}^{1/2} \exp\{j[-\Phi_{\mathrm{DP}}/2 + \Phi_{\mathrm{DP}}^{(t)}]\} + S_{vv}\rangle, \qquad (4)$$

where $A_{hv} = |T_h/T_v|^2$, $\Phi_{\mathrm{DP}} = 1/2[\arg(T_v) - \arg(T_h)]$, and $C'' = C'T_v^2$ depends on the radar parameters and the distance from the radar.

In addition to the standard polarimetric variables routinely measured in the SHV mode, it is suggested that the ratio

$$D_r = \frac{P_h + P_v - 2|R_{hv}|}{P_h + P_v + 2|R_{hv}|} \qquad (5)$$

can serve as a proxy for CDR (Melnikov and Matrosov 2013; Ryzhkov et al. 2014). Equation (5) can be rewritten as

$$D_r = \frac{1 + Z_{\mathrm{dr}}^{-1} - 2\rho_{hv} Z_{\mathrm{dr}}^{-1/2}}{1 + Z_{\mathrm{dr}}^{-1} + 2\rho_{hv} Z_{\mathrm{dr}}^{-1/2}}, \qquad (6)$$

where

$$Z_{\mathrm{dr}} = P_h/P_v \qquad (7)$$

is the measured differential reflectivity expressed in linear scale and

$$\rho_{hv} = |R_{hv}|/(P_h P_v)^{1/2} \qquad (8)$$

is the measured copolar correlation coefficient. It is important to emphasize that the values of Z_{dr} and ρ_{hv} measured in the SHV mode are generally affected by cross coupling between the H and V polarizations and are not identical to the intrinsic Z_{dr} and ρ_{hv} (Z'_{dr} and ρ'_{hv}) defined through the elements S_{hh}, S_{vv}, and S_{hv} of the covariance scattering matrix as

$$Z'_{\mathrm{dr}} = \frac{\langle |S_{hh}|^2 \rangle}{\langle |S_{vv}|^2 \rangle} \quad \text{and} \qquad (9)$$

$$\rho'_{hv} = \frac{|\langle S_{hh}^* S_{vv} \rangle|}{\langle |S_{hh}|^2 \rangle^{1/2} \langle |S_{vv}|^2 \rangle^{1/2}}. \qquad (10)$$

In Eqs. (9) and (10), angular brackets mean averaging over an ensemble of hydrometeors. Additionally, the measured value of Z_{dr} is generally biased because of differential attenuation [factor A_{hv} in Eqs. (3) and (4)]. As can be deduced from Eqs. (3) and (4) containing cross-polarization term S_{hv}, the apparent values of Z_{dr} and ρ_{hv} in Eqs. (7) and (8) depend to some extent on the linear depolarization ratio L_{dr}, and the magnitude of ρ_{hv} is also dependent on the system differential phase upon transmission $\Phi_{\mathrm{DP}}^{(t)}$, that is, the polarization state of the transmitted wave. None of the existing operational dual-polarization radars have the capability to control the polarization state of the transmitted wave.

Using Eqs. (1), (3), and (4), the ratio D_r in Eq. (5) can be expressed via the intrinsic values of Z'_{dr} and ρ'_{hv} as (Ryzhkov et al. 2014)

$$D_r \approx \frac{1 + (Z''_{\mathrm{dr}})^{-1} - 2\rho'_{hv}(Z''_{\mathrm{dr}})^{-1/2} + 4L''_{\mathrm{dr}} \sin^2[\Phi_{\mathrm{DP}}/2 - \Phi_{\mathrm{DP}}^{(t)}]}{1 + (Z''_{\mathrm{dr}})^{-1} + 2\rho'_{hv}(Z''_{\mathrm{dr}})^{-1/2} + 4L''_{\mathrm{dr}} \cos^2[\Phi_{\mathrm{DP}}/2 - \Phi_{\mathrm{DP}}^{(t)}]}, \qquad (11)$$

where

$$Z''_{\mathrm{dr}} = Z'_{\mathrm{dr}} A_{hv} \quad \text{and} \qquad (12)$$

$$L''_{\mathrm{dr}} = L'_{\mathrm{dr}} A_{hv}^{1/2} = \frac{\langle |S_{hv}|^2 \rangle}{\langle |S_{hh}|^2 \rangle} A_{hv}^{1/2}. \qquad (13)$$

Equation (11) is obtained by assuming that the mean canting angle of hydrometeors is equal to zero (i.e., the moments $\langle S_{hh} \times S_{hv} \rangle$ and $\langle S_{vv} \times S_{hv} \rangle$ vanish) and $L'_{\mathrm{dr}} \ll 1$. This assumption, however, may not be valid in the areas of crystals canted in the presence of strong electric fields (Ryzhkov and Zrnić 2007).

Jameson (1987) showed that the circular depolarization ratio can be written in terms of linear polarization parameters as

$$C_{\mathrm{dr}} = \frac{1 + Z'_{\mathrm{dr}} - 2(Z'_{\mathrm{dr}})^{1/2} \rho'_{hv} \cos(\Phi_{\mathrm{DP}}) + 4L'_{\mathrm{dr}} Z'_{\mathrm{dr}}}{1 + Z'_{\mathrm{dr}} + 2(Z'_{\mathrm{dr}})^{1/2} \rho'_{hv} \cos(\Phi_{\mathrm{DP}})}. \qquad (14)$$

Accounting for differential attenuation effects, we get

$$C_{\mathrm{dr}} = \frac{1 + (Z''_{\mathrm{dr}})^{-1} - 2\rho'_{hv}(Z''_{\mathrm{dr}})^{-1/2} \cos(\Phi_{\mathrm{DP}}) + 4L''_{\mathrm{dr}}}{1 + (Z''_{\mathrm{dr}})^{-1} + 2\rho'_{hv}(Z''_{\mathrm{dr}})^{-1/2} \cos(\Phi_{\mathrm{DP}})}. \qquad (15)$$

It is obvious from Eq. (15) that C_{dr} in Eq. (15) is strongly affected by differential phase (i.e., propagation effects), which is a major obstacle to the practical utilization of circular depolarization ratio. Comparing Eq. (11) for D_r and Eq. (15) for C_{dr}, it follows that D_r is very close to C_{dr} for small values of Φ_{DP} if $\Phi_{\mathrm{DP}}^{(t)} = \pm 90°$, that is, when the radar transmits a circularly polarized wave. In this case,

$$D_r = \frac{1 + (Z''_{\mathrm{dr}})^{-1} - 2\rho'_{hv}(Z''_{\mathrm{dr}})^{-1/2} + 4L''_{\mathrm{dr}} \cos^2(\Phi_{\mathrm{DP}}/2)}{1 + (Z''_{\mathrm{dr}})^{-1} + 2\rho'_{hv}(Z''_{\mathrm{dr}})^{-1/2} + 4L''_{\mathrm{dr}} \sin^2(\Phi_{\mathrm{DP}}/2)}. \qquad (16)$$

Moreover, Eqs. (15) and (16) become identical if $\Phi_{\mathrm{DP}} = 0$. If, however, the transmitted wave has a slant 45° linear polarization [i.e., $\Phi_{\mathrm{DP}}^{(t)} = 0°$], then

$$D_r = \frac{1 + (Z''_{\mathrm{dr}})^{-1} - 2\rho'_{hv}(Z''_{\mathrm{dr}})^{-1/2} + 4L''_{\mathrm{dr}} \sin^2(\Phi_{\mathrm{DP}}/2)}{1 + (Z''_{\mathrm{dr}})^{-1} + 2\rho'_{hv}(Z''_{\mathrm{dr}})^{-1/2} + 4L''_{\mathrm{dr}} \cos^2(\Phi_{\mathrm{DP}}/2)}, \qquad (17)$$

and the terms containing L_{dr} have a much smaller impact on D_r than in Eq. (16) provided that Φ_{DP} is relatively small so that $\sin(\Phi_{\mathrm{DP}}/2) \approx 0$. In that case, D_r might be quite different from C_{dr}.

The difference resulting from the transmitted wave being circularly or linearly polarized can be illustrated for randomly oriented hydrometeors. Then

$$\rho'_{hv} = 1 - 2L_{\mathrm{dr}}, \qquad (18)$$

and $Z'_{\mathrm{dr}} = 1$ (Bringi and Chandrasekar 2001). It can be easily shown that $D_r \approx 2L_{\mathrm{dr}}$ and $D_r = L_{\mathrm{dr}}$ for circularly and linearly polarized transmitted waves, respectively, provided that $\Phi_{\mathrm{DP}} = 0$. In the former case, D_r is equal to C_{dr}, and in the latter case, it is about 3 dB lower. A more detailed analysis for different types of hydrometeor orientation and various polarizations of the transmitted wave (generally elliptical) indicates that the highest values of DR are achieved for circular polarization of the transmitted wave although the variability of DR with $\Phi_{\mathrm{DP}}^{(t)}$ does not exceed 3 dB (if the mean canting angle of hydrometeors is equal to 0°). One has to keep in mind that the impact of antenna cross coupling on the quality of the measurements of polarimetric radar variables is maximized if the polarization of the transmitted wave is circular (Hubbert and Bringi 2003; Wang and Chandrasekar 2006; Wang et al. 2006; Hubbert et al. 2010). The biases in Z_{DR}, ρ_{hv}, and Φ_{DP} are also highest for circular polarization on transmission if the mean canting angle is different from zero (Ryzhkov and Zrnić 2007). However, if the antenna cross talk is small and the mean canting angle of hydrometeors is close to zero (which is generally a valid assumption except for low-inertia ice crystals in electrically active zones of clouds), then the use of circular polarization upon transmission (i.e., $\Phi_{\mathrm{DP}}^{(t)} = \pm 90°$) has an advantage in maximizing depolarization ratio DR. Anyway, the depolarization ratio D_r defined by Eq. (11) contains information useful for the discrimination between different types of ice and mixed-phase hydrometeors even if the polarization of the transmitted wave is not circular, as will be shown in the next sections.

It is important to note that D_r is much less affected by the propagation differential phase than C_{dr}, which is a great advantage of D_r. Both D_r and C_{dr} are, however, affected by another propagation effect, differential attenuation, which is described by the factor A_{hv} in Eqs. (12) and (13). Therefore, the advantage of measuring D_r instead of C_{dr} is greater at longer radar wavelengths where attenuation/differential attenuation in rain is smaller.

3. Simulations based on experimental data

Our theoretical analysis demonstrates that the depolarization ratio, $\mathrm{DR} = 10\log_{10}(D_r)$, which serves as a good proxy for the circular depolarization ratio CDR, can be estimated by radars with simultaneous transmission/reception along with the standard set of polarimetric variables Z_{DR}, ρ_{hv}, and Φ_{DP}. The best correspondence between DR and the "true" CDR is achieved if the radar transmits the wave with circular polarization, which means that the differential phase upon transmission $\Phi_{DP}^{(t)}$ is equal to $\pm 90°$. The implementation of DR measurements requires the computation following Eq. (5) and the control of the polarization of the transmitted wave using a high-power phase shifter in one of the orthogonal transmission channels to maximize DR and make it close to CDR if needed. According to Eq. (15), the circular depolarization ratio CDR can be computed from the measurements of Z_{DR}, ρ_{hv}, and Φ_{DP} only if LDR is also available (which is not the case for operational polarimetric weather radars). For this purpose, we resort to the data collected by the National Center for Atmospheric Research (NCAR) research S-band dual-polarization Doppler radar (S-Pol), which measured all needed variables. A thunderstorm in Florida on 14 August 1998 is selected for the following analysis, a case already examined in the paper by Ryzhkov et al. (2002).

An example of vertical cross sections of the measured Z, Z'_{DR}, ρ'_{hv}, LDR, Φ_{DP}, and the estimates of two depolarization ratios is displayed in Fig. 1 for the azimuth angle 172.2°. The first depolarization ratio (tagged as CDR) is obtained from Eq. (15) and represents what would be measured by a true circularly polarized radar. The impact of propagation (or Φ_{DP}) on CDR is obvious: the intrinsic CDR is grossly overestimated in areas with even modest Φ_{DP} values (up to 10°–20°). Such an overestimation is expected to be much more dramatic at shorter radar wavelengths where Φ_{DP} is larger. Different approaches for correcting CDR for differential phase shift were discussed in the literature (e.g., Torlaschi and Holt 1993, 1998), but none proved to be efficient.

The second estimate of DR is computed from Eq. (16) for D_r, which is obtained by assuming that $\Phi_{DP}^{(t)} = \pi/2$ in Eq. (11). This depolarization ratio is not affected by propagation while being very consistent with intrinsic CDR (in the absence of the propagation impact) and results of theoretical simulations, which can be found in literature (Jameson 1987; Al-Jumily et al. 1991; Torlaschi and Holt 1993, 1998; Holt et al. 1999; Matrosov et al. 2001, 2012). The DR seems to be more informative for hydrometeors above the melting layer than the traditionally utilized Z_{DR} and ρ_{hv} and thus may complement other polarimetric measurements. The microphysical interpretation of DR is less ambiguous than deciphering LDR because the latter depends on particle shape, density, and orientation, whereas DR serves as a proxy for true CDR, which is only weakly affected by orientation. For example, DR allows distinguishing between the updraft associated with the Z_{DR} column centered at $R = 20$ km and the nearby downdraft filled with nearly spherical dry graupel particles centered at $R = 23$ km above the freezing level, whereas LDR does not. This is mainly because raindrops lofted in a convective updraft are relatively well oriented, which reduces LDR despite their quite nonspherical shape. The DR exhibits a very pronounced signature in the melting layer and offers a valuable resource for polarimetric microphysical retrievals.

Vertical cross sections of Z, Z'_{DR}, ρ'_{hv}, LDR, DR, and Φ_{DP} for the same case but for a different azimuth (184.2°) in a more stratiform part of the storm are displayed in Fig. 2. Again, as in Fig. 1, Z'_{DR} and ρ'_{hv} above the melting layer do not reveal pronounced patterns or signatures, whereas both LDR and DR exhibit a coherent structure in the ice part of the storm. Obviously, DR correlates well with LDR while being a few dB higher.

The value of DR displayed in Figs. 1 and 2 is computed from Eq. (11) assuming that the polarization of the transmitted wave is circular [$\Phi_{DP}^{(t)} = 90°$]. We examined the influence of $\Phi_{DP}^{(t)}$ on the estimated DR and compare the DR cross sections with $\Phi_{DP}^{(t)}$ changing from 90° to 20° (Fig. 3) with a 10° increment. It is evident that the highest DR corresponds to $\Phi_{DP}^{(t)} = 90°$ (i.e., the transmitted wave is circularly polarized) and gradually decreases with $\Phi_{DP}^{(t)}$ approaching 0°.

Vertical profiles of DR, LDR, and ρ_{hv} through the melting layer at $Az = 184.2°$ and a distance of 18 km from the radar are displayed in Fig. 4. The quantities LDR and DR are well correlated above the melting layer. Within the melting layer, the DR's pronounced maximum coincides with the ρ_{hv} minimum, whereas LDR increases monotonically with height. As expected, DR in rain is much higher than LDR. The difference between ρ_{hv} in pure rain below the melting layer and frozen hydrometeors above it is vanishingly small, whereas DR in rain is very different from DR above the melting layer.

Ryzhkov (2001) showed that the difference between CDR and LDR depends primarily on particle orientations, so joint measurements of different depolarization ratios can be used to infer hydrometeor fall attitudes (e.g., Matrosov et al. 2005). If the hydrometeors are oriented randomly, then the difference CDR − LDR is roughly 3 dB and does not depend on the radar elevation angle as mentioned previously and is visible in many regions above the melting layer in the figures shown. For relatively narrow distributions of the canting angles,

$$\frac{C_{dr}}{L_{dr}} \approx \frac{\langle |s_h|^2 \rangle}{\langle |s_h + s_v|^2 \rangle} \frac{1}{\sigma^2 + \langle \alpha \rangle}, \quad (19)$$

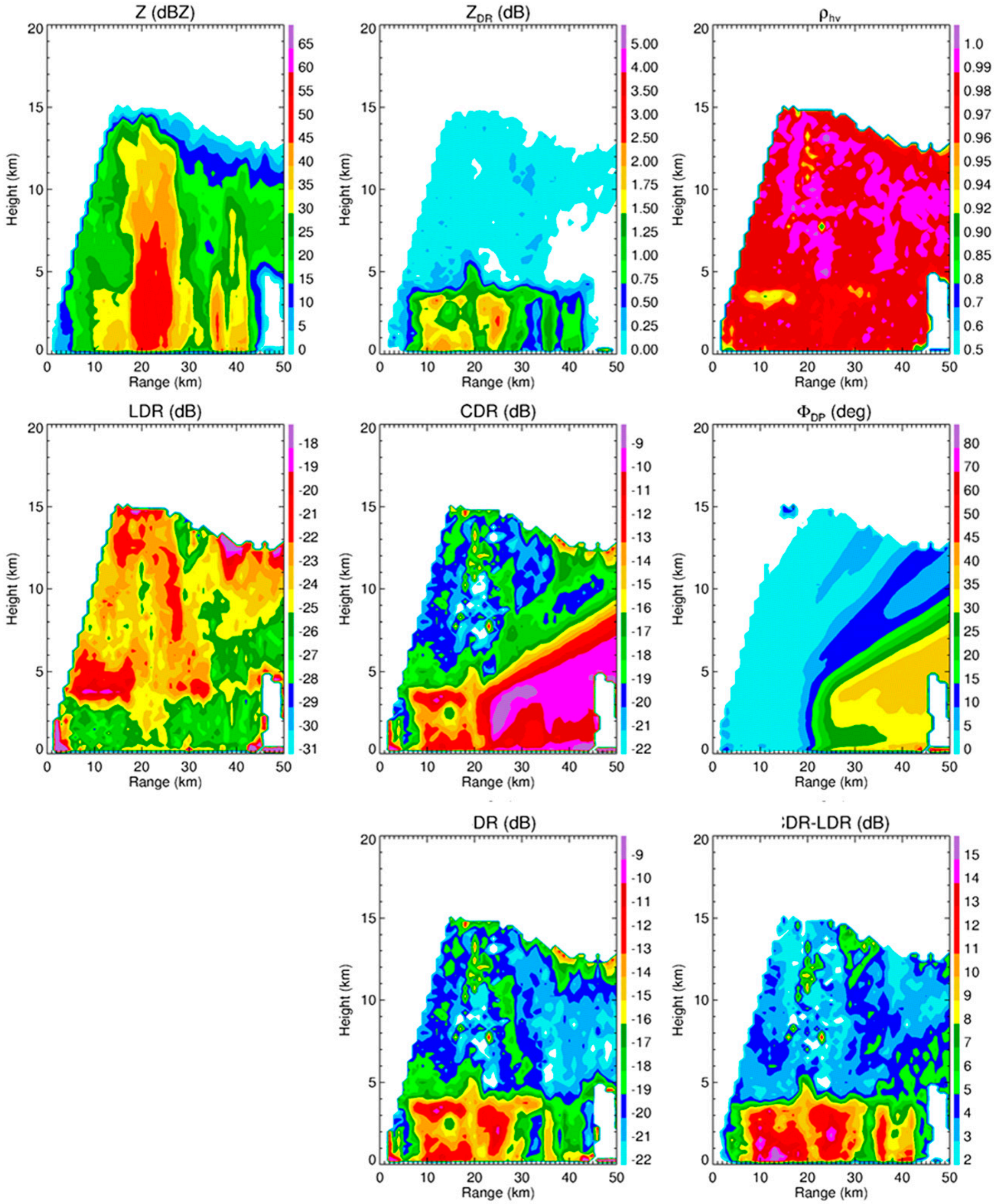

FIG. 1. Vertical cross section of Z_e, Z'_{DR}, ρ'_{hv}, LDR, CDR, Φ_{DP}, DR, and DR − LDR for the case on 14 Aug 1998, at azimuth = 172.2°. The data are collected by the NCAR S-Pol radar. The CDR is retrieved from the measured Z'_{DR}, LDR, ρ'_{hv}, and Φ_{DP} using Eq. (15) assuming that system differential phase $\Phi_{\mathrm{DP}}^{(t)} = 90°$. The DR is retrieved from Eq. (11) with $\Phi_{\mathrm{DP}}^{(t)} = 90°$.

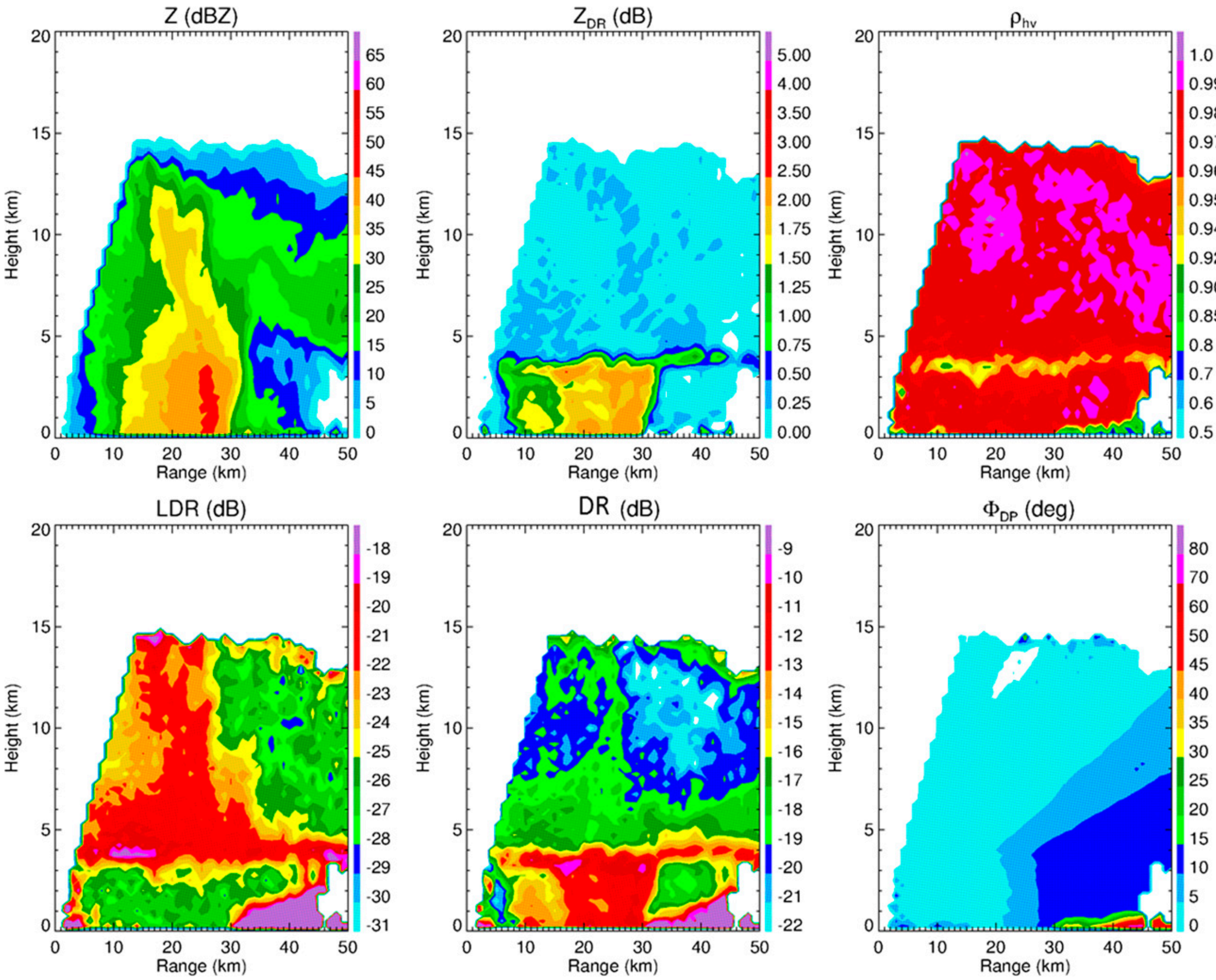

FIG. 2. Vertical cross section of Z, Z'_{DR}, ρ'_{hv}, LDR, DR computed from Eq. (11) with $\Phi_{\mathrm{DP}}^{(t)} = \pi/2$, and Φ_{DP} for the case on 14 Aug 1998 at azimuth = 184.2°. The data are collected by the NCAR S-Pol radar.

where s_h and s_v are the scattering amplitudes in orthogonal directions, $\langle\alpha\rangle$ is the mean canting angle, and σ is the width of the canting angle distribution. In rain, $\langle\alpha\rangle \approx 0$, and the factor containing s_h and s_v varies between 0.25 and 0.35; hence, the ratio $C_{\mathrm{dr}}/L_{\mathrm{dr}}$ (or the difference CDR − LDR expressed in dB) is a measure of σ. In the examples shown in Figs. 1 and 2, DR − LDR varies between 10 and 15 dB in rain below the melting layer. This corresponds to σ varying between 5° and 10° in full agreement with the disdrometer studies (Huang et al. 2008). This is another evidence indicating that our procedure yields realistic estimates of CDR using DR as its proxy.

In general, DR positively correlates with Z_{DR}, and such correlation is much stronger in rain than in snow. This is illustrated in Fig. 5, where the scatterplots of DR versus Z_{DR} in rain below the melting layer (blue dots) and ice/snow above the melting layer (red dots) estimated for two values of $\Phi_{\mathrm{DP}}^{(t)}$ ($\pi/2$ and 0) are displayed for the S-Pol case. The DR in snow/ice is noticeably higher than in rain for a given Z_{DR}. Another important conclusion from Fig. 5 is that using circular polarization on transmission [$\Phi_{\mathrm{DP}}^{(t)} = \pi/2$] instead of slant linear polarization [$\Phi_{\mathrm{DP}}^{(t)} = 0$] results in a higher DR and a better discrimination between rain and ice in the Z_{DR}–DR plane. This emphasizes the value of the phase shifter to control the polarization of the transmitted wave in order to ensure maximal values of DR.

In the previous examples, CDR and its proxy DR were computed from the radar variables (i.e., Z'_{DR}, ρ'_{hv}, LDR, and Φ_{DP}). In the next example, CDR and DR are estimated directly from the in-phase and quadrature components I and Q of the radar signals (Doviak and Zrnić 1993) measured by the polarimetric S-band KOUN WSR-88D in Norman, Oklahoma, following Eq. (5). Figure 6 shows

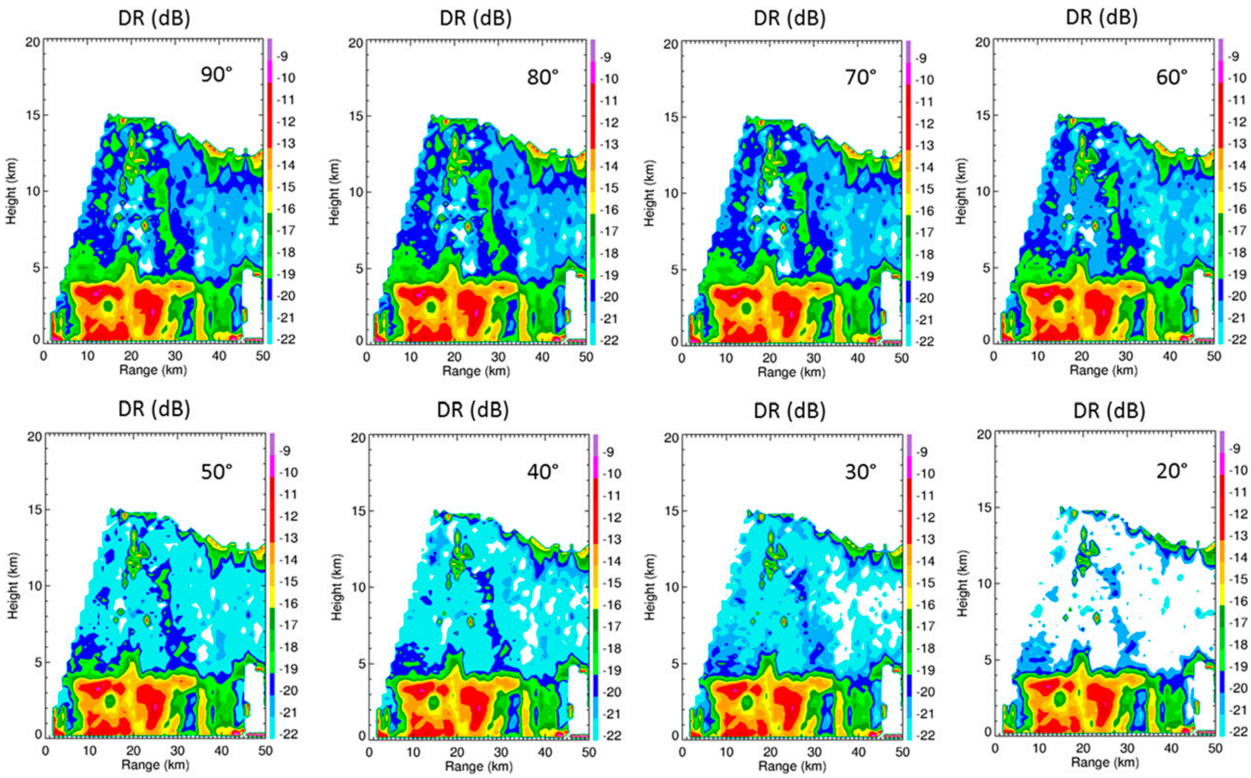

FIG. 3. Vertical cross sections of estimated DR for different values of system differential phase on transmission $\Phi_{DP}^{(t)}$ ranging from 90° (ideal setting) to 20° at the azimuth 172.2°. The data are collected by the NCAR S-Pol radar on 14 Aug 1998.

composite range–height indicators (RHIs) of Z, Z_{DR}, Φ_{DP}, LDR, CDR, and DR for the storm observed on 3 July 2007. The quantities Z, Z_{DR}, Φ_{DP}, CDR, and DR are estimated in the SHV mode of operation, while LDR is measured in the LDR mode whereby only the H-polarized wave is transmitted. The system differential phase on transmission $\Phi_{DP}^{(t)}$ was about 82° at the time of measurements. This means that the polarization of the transmitted wave in the SHV mode was very close to circular. Again, DR estimated from Eq. (11) does not exhibit a bias attributed to propagation differential phase.

4. Direct measurements of DR with a prototype of an operational radar

The suggested methodology for DR measurements prescribing the use of a high-power phase shifter, and a signal processing according to Eq. (5) has been implemented by the Enterprise Electronics Corporation on its C-band dual-polarization radar with simultaneous transmission/reception in Enterprise, Alabama. The phase shifter controlling the differential phase upon transmission $\Phi_{DP}^{(t)}$ was calibrated using alternate measurements of differential phase in the SHV and LDR modes in rain at ranges close to the radar. The estimated system differential phase in the SHV mode of operation is equal to the sum of $\Phi_{DP}^{(t)}$ and $\Phi_{DP}^{(r)}$, whereas it

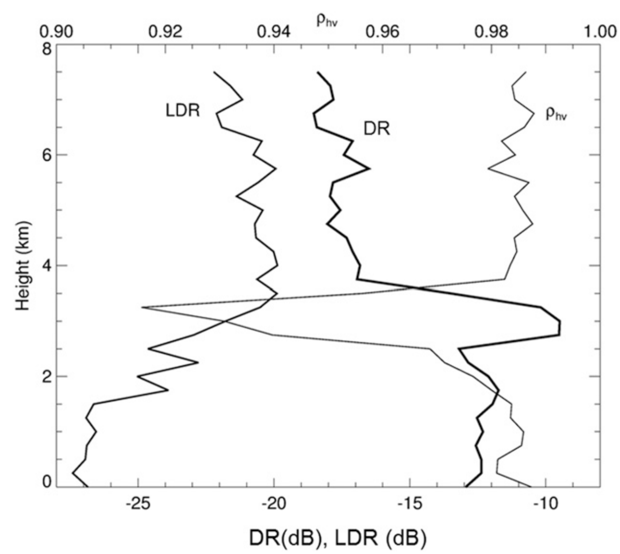

FIG. 4. Vertical profiles of DR, LDR, and ρ'_{hv} at a distance of 18 km from the radar and at azimuth = 184.2°. The data are collected by the NCAR S-Pol radar on 14 Aug 1998.

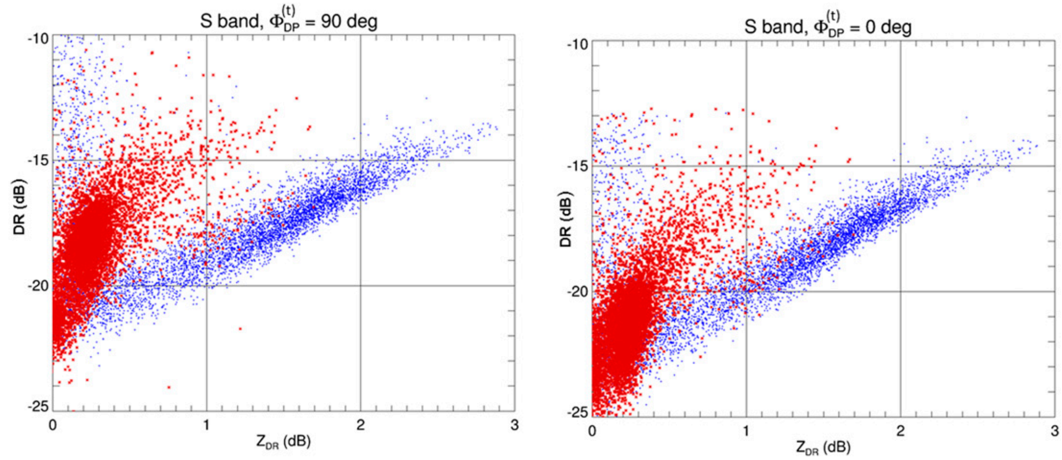

FIG. 5. Scatterplots of DR vs Z_{DR} in rain (blue dots) and ice/snow (red dots) estimated at S band on 14 Aug 1998 for two values of $\Phi_{\mathrm{DP}}^{(t)}$: 90° and 0°.

is equal to $\Phi_{\mathrm{DP}}^{(r)}$ in the LDR mode. Subtracting the two yields the estimate of $\Phi_{\mathrm{DP}}^{(t)}$. The shifter was tuned to achieve $\Phi_{\mathrm{DP}}^{(t)} = 90°$.

The quality of DR measurements can be evaluated using the expected consistency between DR and Z_{DR} in pure rain. Figure 7 (left panel) shows the scatterplot of DR versus Z'_{DR} in rain simulated from a large dataset of disdrometer measurements in central Oklahoma (Schuur et al. 2005). The DR was computed using Eq. (16) with $\Phi_{\mathrm{DP}} = 0$ from simulated Z'_{DR}, ρ'_{hv}, and LDR at C band, assuming that the width of the canting angle distribution is 10°. The scatterplot of DR versus Z_{DR} obtained from measured C-band data collected in stratiform rain in Alabama on 25 February 2015 is presented in the top right panel in Fig. 7. It is consistent with the scatterplot of the simulated values in the left panel (at least for $Z_{\mathrm{DR}} > 0.5$ dB). Observed DR for $Z_{\mathrm{DR}} < 0.5$ dB corresponding to the areas dominated by small quasi-spherical raindrops are higher than the theoretical ones. This can be attributed to antenna cross coupling in the SHV mode. A possible impact of noise can also not be excluded, although the noises in the two orthogonal channels were subtracted from the measured powers before using Eq. (5). The scatterplot of DR versus Z_{DR} in ice above the melting layer for the same event exhibits generally higher values of DR than in the rain below the melting layer for a given Z in full agreement with the estimates from the S-Pol measurements displayed in Fig. 5. The fact that raindrops are well oriented with the width of the canting angle distribution within a 5°–10° range makes DR and Z_{DR} tightly correlated in rain. This is not the case in snow and ice, where the two variables are less correlated because of a more random orientation of snowflakes and ice crystals. Indeed, dry snow aggregates have nonspherical shape, but their Z_{DR} is close to zero because of their low density.

Average vertical profiles of Z, Z_{DR}, ρ_{hv}, and DR obtained via azimuthal averaging of these variables at elevation 15° for the above case are shown in Fig. 8. The depolarization ratio has a pronounced maximum within the melting layer with DR approaching −16 dB. Additionally, DR exhibits a small bump at about 6-km height within the dendritic growth layer in the temperature interval between −10° and −20°C, which is also marked by an increase in Z_{DR} (e.g., Kennedy and Rutledge 2011; Williams et al. 2015). Overall, the depolarization ratio for this winter stratiform event is lower than DR estimated from the S-Pol for a convective summer storm at all heights, as the comparison of Figs. 4 and 8 demonstrates. Further scrutiny is required to explain these differences.

In deep convective storms, the linear depolarization ratio LDR has been traditionally used for hail detection above the freezing level (e.g., Barge 1974; Bringi et al. 1986; Holler et al. 1994; Carey and Rutledge 1998; Hubbert et al. 1998; Kennedy et al. 2001). Kennedy et al. (2001) suggest an S-band LDR threshold of −25 dB at mid- to upper levels of a thunderstorm for the detection of growing hail. Hail growth in the convective updrafts is often seen as an ‘‘LDR cap’’ on the top of the Z_{DR} column, which is aligned with the base of such updrafts (Jameson et al. 1996; Bringi et al. 1997; Hubbert et al. 1998; Carey and Rutledge 1998; Kumjian et al. 2014).

The depolarization ratio DR was estimated with the Enterprise Electronics Corporation (EEC) C-band radar data using Eq. (5) in a hail-bearing storm in Alabama on 7 August 2015. Figure 9 displays composite RHI and plan

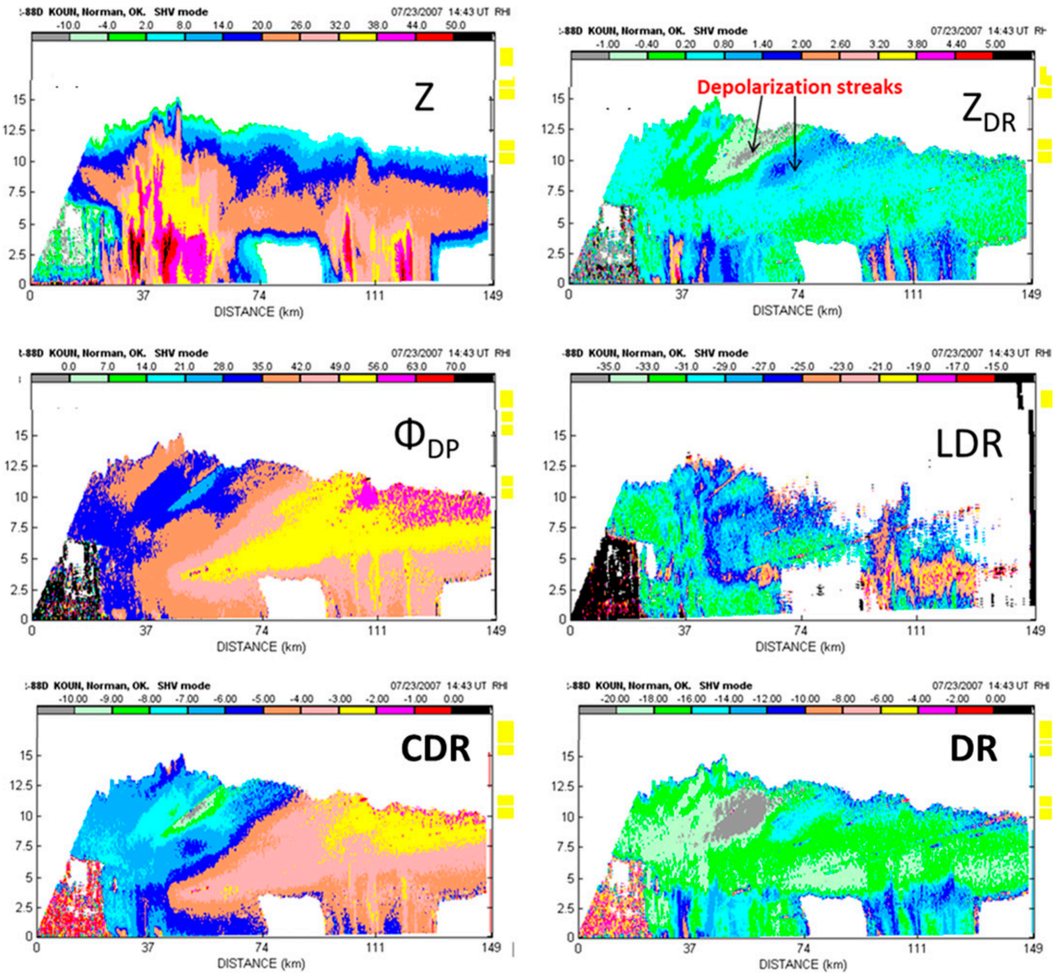

FIG. 6. Composite RHI of Z, Z_{DR}, Φ_{DP}, LDR, CDR, and DR retrieved from I and Q data collected by the KOUN WSR-88D on 3 Jul 2007. The quantities Z, Z_{DR}, Φ_{DP}, CDR, and DR are measured in the SHV mode of operation. The LDR is measured in the LDR mode when only the wave with horizontal polarization is transmitted.

position indicator (PPI) plots of Z, Z_{DR}, ρ_{hv}, and DR for a convective cell containing hail aloft. The RHI scans were reconstructed from the series of successive PPI sweeps; thus, their vertical resolution is somewhat compromised. Nevertheless, the convective cell with maximal reflectivity of 58 dBZ is marked by a well-pronounced Z_{DR} column and a much taller column of DR with a maximal value as high as -10 dB, which is indicative of wet, large hail growing in the convective updraft. Obviously, the DR column can better indicate a strong convective updraft than the Z_{DR} column. Indeed, the DR column seems to combine the base of updraft where Z_{DR} is high because of the presence of large liquid or partially frozen raindrops and the LDR cap in the middle or at the top of updraft where water-coated or spongy hail is growing in a wet growth regime. Therefore, DR can potentially be used for hail detection aloft and for the estimation of its size (e.g., Mirkovic 2016). The composite PPIs of Z, Z_{DR}, and DR at different antenna elevations (and thus heights) in Fig. 10 demonstrate that the updraft signatures in terms of Z_{DR} disappear at 7 km, whereas the DR column is still clearly detectable up to 9 km.

5. Potential practical utilization of DR

Three major challenging practical tasks can be addressed using DR measurements: 1) detection of hail and determination of its size above the melting layer, 2) differentiating between various ice habits aloft, and 3) quantification of riming associated with the presence of supercooled cloud water hinting at potential icing hazard for airplanes. These are addressed next.

a. *Detection of hail and estimation of its size*

The hail size discrimination algorithm (HSDA) recently developed at NSSL for implementation on the

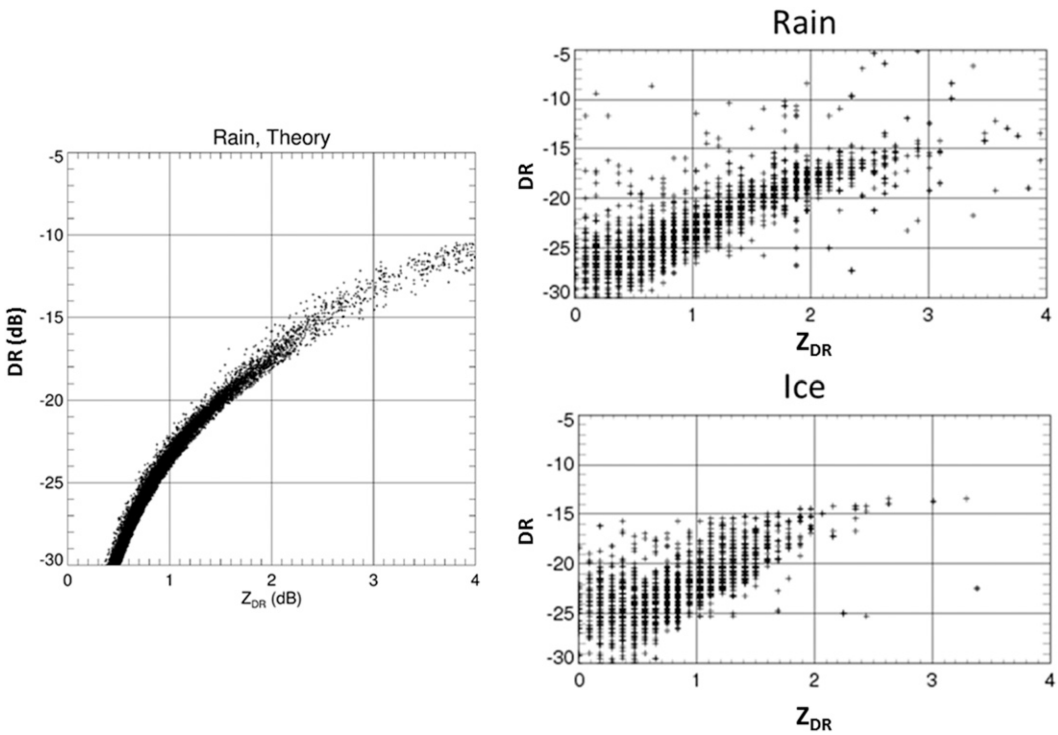

FIG. 7. Scatterplots of (left) simulated and (right) measured values of DR vs Z_{DR} in (top) rain and (bottom) ice/snow for the event on 25 Feb 2015 observed by the EEC C-band dual-polarization radar. The DR in the right panels is estimated using Eq. (5).

WSR-88D network distinguishes between small ($D <$ 2.5 cm), large ($2.5 < D < 5.0$ cm), and giant ($D > 5.0$ cm) hail (Ryzhkov et al. 2013b; Ortega et al. 2016). The algorithm capitalizes primarily on polarimetric signatures below the melting layer, where melting hail is mixed with rain. This implies that hail has already been formed aloft and falls to the ground. For hail nowcasting and suppression, however, it is important to detect large hail earlier, when it is just formed in the upper part of the storm where radar reflectivity Z is a primary discrimination parameter in HSDA and where differential reflectivity Z_{DR} is usually close to zero. In contrast, both LDR and CDR (or DR) above the freezing level vary significantly depending on hail size and shape. Simulations of CDR based on the microphysical model of hail described in Ryzhkov et al. (2013a) and Mirkovic (2016) show that CDR can increase by about 10 dB if the maximal diameter of dry hail changes from 8 to 50 mm. In computations, it was assumed that the width of the mean canting angle distribution is equal to 40°, and the aspect ratio of hailstones is 0.8 if their size exceeds 1 cm and varies between 0.8 and 1.0 for smaller sizes as specified in Ryzhkov et al. (2011).

The steady increase of CDR with the maximal hail size is caused by progressively stronger resonance scattering effects for larger hailstones and by the decrease of the slope of the exponential size distribution in case of larger hail (Aydin and Zhao 1990; Ryzhkov et al. 2013a). Very big hail with diameters larger than 5 cm usually grows in a wet growth regime and may have quite significant water fraction even at negative temperatures while residing in a convective updraft. The magnitude of dielectric constant for wet hail is higher than for dry hail, which results in higher Z_{DR}, LDR, CDR, and lower ρ_{hv}.

The utilization of the DR column discussed in the previous section offers an additional opportunity to identify large or giant hail growing in a wet growth regime within the convective updraft. As was mentioned in section 2, the depolarization ratio DR best approximates the true circular depolarization ratio CDR (unbiased by the impact of differential phase) if the polarization of the transmitted wave is circular. Then the value of DR and its discriminatory power are highest (see Fig. 3). However, we believe that the depolarization ratio derived from SHV radar measurements can be also useful for arbitrary polarization of the transmitted wave, which is the case for the majority of existing operational and research dual-polarization radars. Moreover, the depolarization ratio computed from the measured Z_{DR} and ρ_{hv} using Eq. (6) may provide new insights into the microphysical

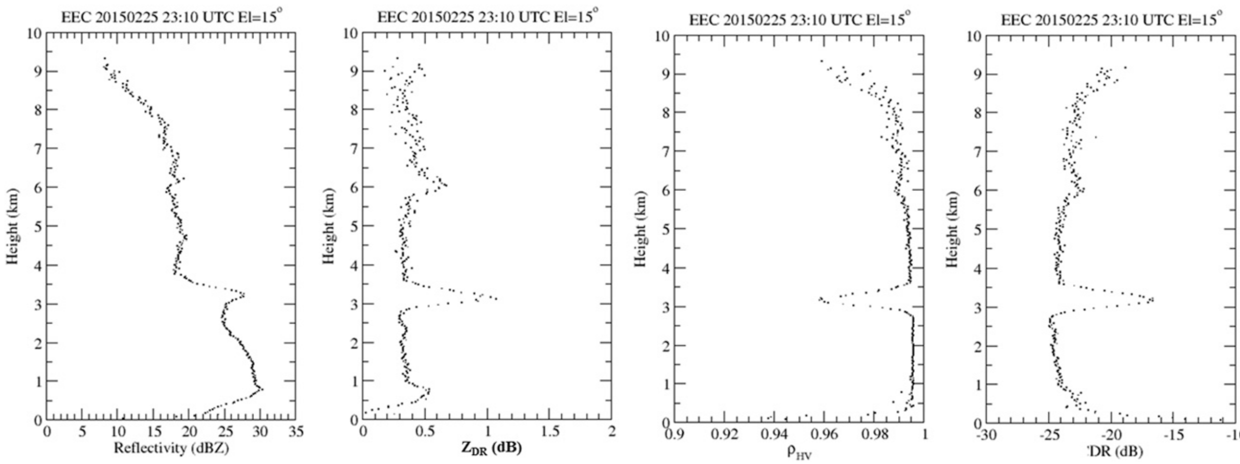

FIG. 8. Vertical profiles of Z, Z_{DR}, ρ_{hv}, and DR through the melting layer obtained by azimuthal averaging of the radar variables at elevation = 15° observed at 1826 UTC 25 Feb 2015 by the EEC C-band dual-polarization radar. The DR is estimated using Eq. (5).

properties of frozen and mixed-phase hydrometeors because it combines the information contained in Z_{DR} and ρ_{hv} in a single signature or feature. To demonstrate this, we examined several weather events observed with dual-polarization radars for which the differential phase upon transmission $\Phi_{DP}^{(t)}$ was not known.

A hailstorm producing large hail in central Oklahoma on 17 June 2005 was observed by the KOUN S-band radar, which served as a prototype of the operational dual-polarization WSR-88D sets. The radar antenna was scanning in the vertical plane at a number of azimuthal directions within a narrow azimuthal sector so that high-resolution RHIs have been produced. Examples of the composite RHIs of Z, Z_{DR}, ρ_{hv}, and DR computed from Z_{DR} and ρ_{hv} are shown in Figs. 11 and 12.

A classical signature of melting hail falling toward the ground is displayed in Fig. 11. It is centered at range 75 km

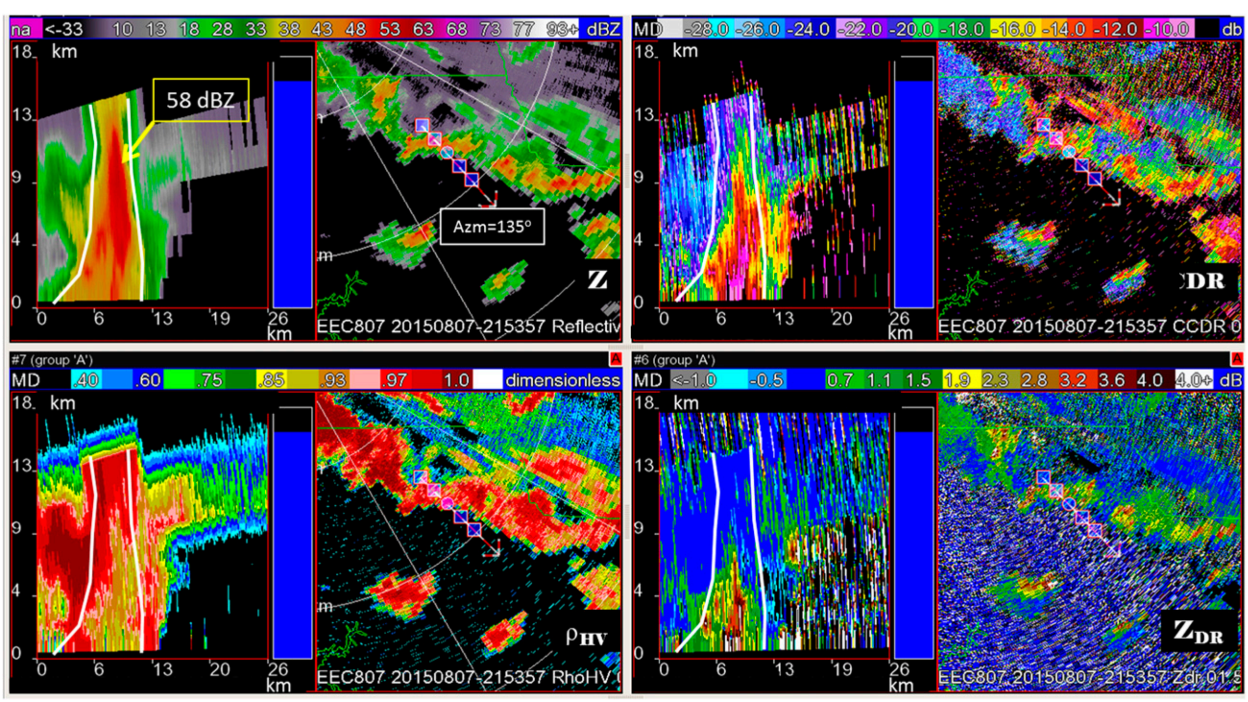

FIG. 9. Composite RHI and PPI of Z, Z_{DR}, ρ_{hv}, and DR measured by the C-band EEC dual-polarization radar in a hail-bearing thunderstorm at 2153 UTC 7 Aug 2015. The DR is estimated from Eq. (5).

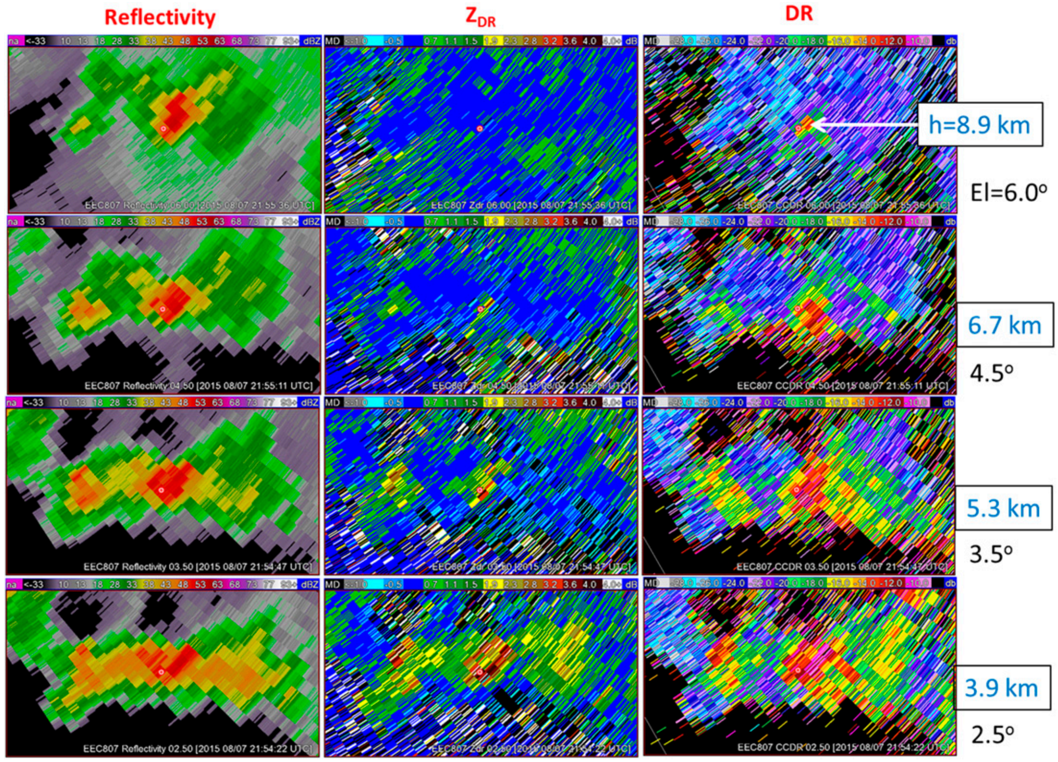

FIG. 10. Composite PPIs of Z, and DR measured by the C-band EEC dual-polarization radar at different antenna elevations at 2154 UTC 7 Aug 2015. The DR is estimated from Eq. (5).

from the radar and marked by high Z (exceeding 60 dBZ next to the surface), low Z_{DR}, and depressed ρ_{hv}. A "Z_{DR} hole" is clearly visible at this range. Of primary interest, however, is the signature of a new convective updraft indicated by a white oval, centered 68 km from the radar. The updraft can be identified by a relatively short Z_{DR} column stretching 1.5 km above the environmental freezing level at 4 km. This updraft is also characterized by a much taller area of ρ_{hv} depression, which is a proxy for an LDR cap. These Z_{DR} and ρ_{hv} signatures are combined in a strong DR column, which is very similar to the one illustrated in Fig. 9. Note that radar reflectivity is very modest in this area, indicating that hailstones growing in the upper part of this updraft are still small.

Figure 12 shows the signature of very large hail observed in the same storm but 40 min later. The hail core centered 35 km from the radar is characterized by very high values of Z exceeding 65 dBZ, very low ρ_{hv} (<0.8), and negative Z_{DR} (as low as -1.3 dB) aloft at the height exceeding 3 km AGL. Negative values of Z_{DR} definitely signal the presence of giant hailstones with diameters larger than 5 cm as a result of resonance scattering, as shown by Ryzhkov et al. (2013a). The combination of anomalously low Z_{DR} and ρ_{hv} yields very high values of DR exceeding -10 dB. The examples in Figs. 11 and 12 demonstrate that combining the Z_{DR} and ρ_{hv} signatures into a single feature, that is, depolarization ratio, may help to better identify large hail aloft and complement traditional reflectivity-based criteria of the vertically integrated liquid (VIL) or maximum expected size of hail (MESH) (Witt et al. 1998).

b. *Identification of different ice particle habits*

Matrosov et al. (2001) and Matrosov (2015) showed that the dependence of the absolute values of CDR [(and/or closely related to it slant 45° linear depolarization ratio (SLDR)] on the antenna elevation angle can be used for the discrimination between different ice hydrometeor habits and the estimation of particle shape parameters (e.g., aspect ratios). The CDR increases with decreasing antenna elevation for planar (oblate) types of snow crystals (hexagonal plates, thick plates, dendrites), whereas the elevation dependency of CDR is relatively "flat" for columnar (prolate) type crystals (columns, needles, etc.). At low elevation angles, CDR varies in a large range (from the radar system depolarization limit to about -8 dB) depending on the ice habit. According to cloud radar observations by Matrosov et al. (2001, 2012), pristine dendrites and hexagonal plates have highest values of CDR up to -8 dB (at slant viewing) followed by

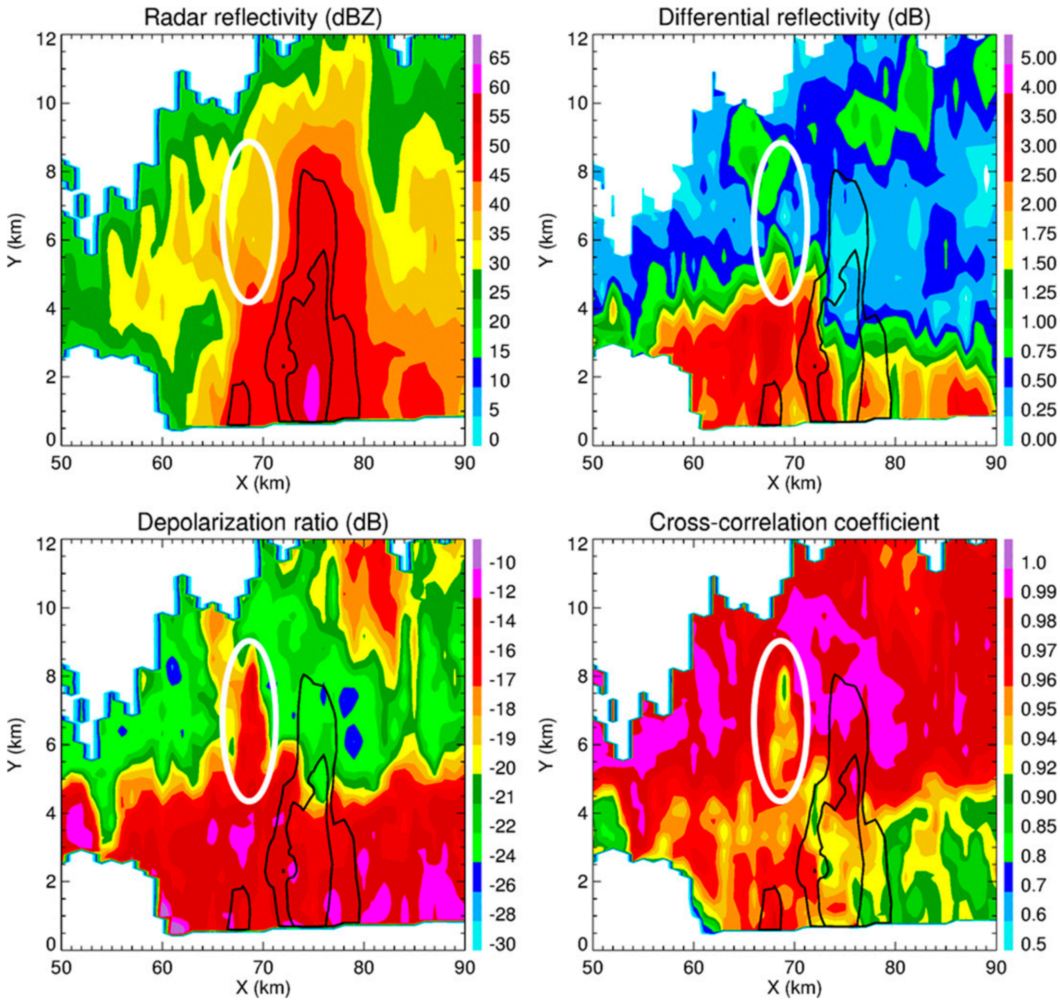

FIG. 11. Composite RHI of Z, Z_{DR}, ρ_{hv}, and DR computed from Z_{DR} and ρ_{hv} using Eq. (6) in a hailstorm observed by the KOUN radar at 0406 UTC 17 Jun 2005 and azimuth = 305°. The white oval encloses a convective updraft of a newly developing cell.

columns and aggregates of dendrites (from −23 to −16 dB) with graupel indicating the lowest CDR below −25 dB. Note that the specific values of actually measured depolarization ratios are affected (especially for lower depolarizations) by the particular radar antenna cross-coupling characteristics. Since the suggested DR parameter represents a CDR proxy, it can be useful for future studies of ice hydrometeor habits.

Another potential application may involve the discrimination between aggregated and rimed snow and possible quantification of the degree of riming. Riming denotes the freezing of small supercooled liquid droplets (with sizes from microns to tens of microns) on faster falling ice crystals and snowflakes. Supercooled liquid water cannot be observed directly by weather surveillance radars because of the small size of liquid droplets, but its presence can be detected indirectly by estimating the degree of riming of ice crystals. Riming tends to increase the density and aspect ratio of ice particles, that is, it makes them denser and more spherical. The density effect increases CDR while the shape effect changes CDR in the opposite direction. Both theoretical and experimental studies backed by in situ particle observations indicate that the shape effect usually dominates so that riming reduces CDR at low elevation angles (e.g., Matrosov et al. 2001, 2012).

c. *Quasi-vertical profiles of depolarization ratio*

Another possible way to discriminate between aggregated and rimed snow implies the use of the concept of quasi-vertical profiles (QVPs) of radar variables including the depolarization ratio DR. Such a concept has been recently introduced by Trömel et al. (2013) and Ryzhkov et al. (2016). It suggests azimuthal

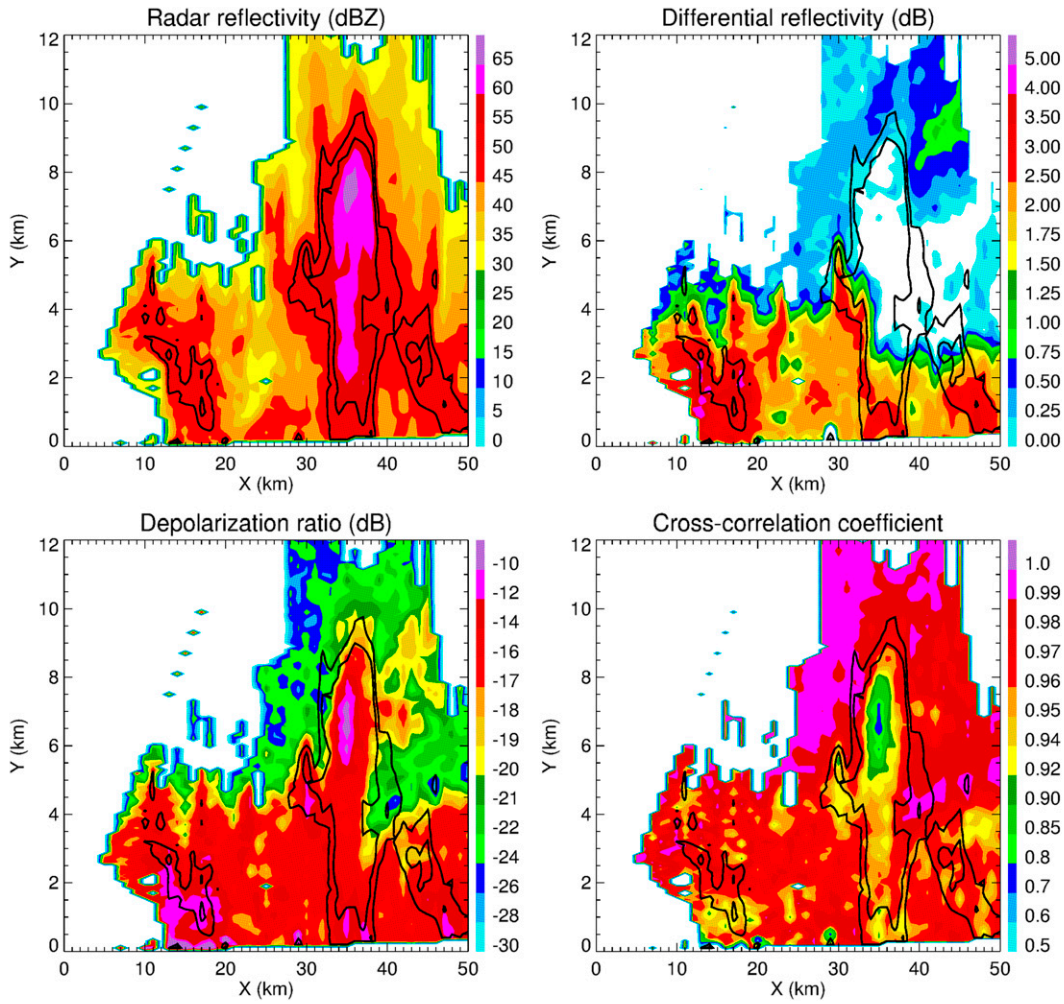

FIG. 12. As in Fig. 11, but for azimuth = 270° at 0447 UTC.

averaging of the radar data on conical scans at high antenna elevations (between 10° and 30°) to reduce the statistical uncertainty of the radar variables estimates. Trömel et al. (2013) demonstrated the QVP strategy as a pathway to reliably estimate the backscatter differential phase in the melting layer. The QVP profiles are represented in a height versus time format, and the evolution of the microphysical processes of snow formation above the freezing level can be captured in relative detail. Since the statistical errors of Z_{DR} and ρ_{hv} in the QVP profiles are very small, Eq. (6) can be effectively used for the computation of QVPs of DR with high accuracy for most dual-polarization radars.

An example of the composite QVP of Z, Z_{DR}, ρ_{hv}, and DR estimated from the KMOB WSR-88D data using Eq. (6) for a winter stratiform event near Mobile, Alabama, is presented in Fig. 13. The QVP methodology allows delineating the melting layer and the dendritic growth layer usually found in the temperature interval between $-10°$ and $-15°$C (or 5–6 km in height) and their temporal evolution with unprecedented accuracy and vertical resolution. The depolarization ratio reaches -15 dB within the melting layer and -19 dB in the dendritic growth layer. The latter is also denoted by strong Z_{DR} enhancement and a reduction of ρ_{hv} (Williams et al. 2015).

In Fig. 13, DR follows the pattern of Z_{DR}, which is not surprising from the physical standpoint and because DR is computed from Z_{DR} and ρ_{hv}. Nevertheless, there are certain differences due to the dependence of DR on ρ_{hv} as well. How close is DR computed from Eq. (6) to the real circular depolarization ratio CDR? This depends on the system differential phase upon transmission $\Phi_{DP}^{(t)}$, which changes from radar to radar on the WSR-88D fleet and generally is not known. Regardless of the difference between DR and true CDR, DR turns out to be a useful radar parameter characterizing microphysical properties

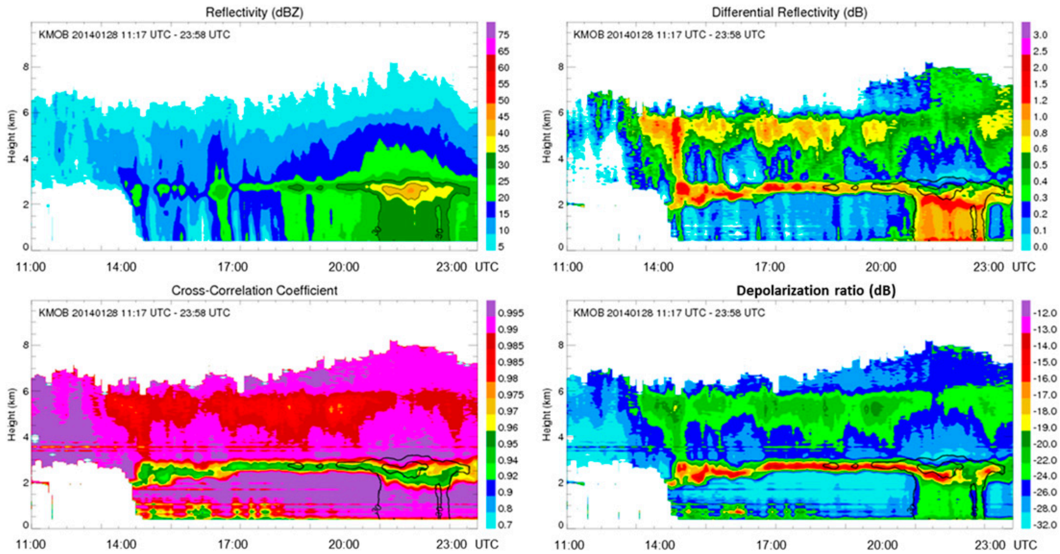

FIG. 13. Composite QVP of Z, Z_{DR}, ρ_{hv}, and DR [estimated from Eq. (6)] obtained from the KMOB WSR-88D at elevation 9.9° on 28 Jan 2014.

of snow. In general, the range of values of DR in Fig. 13 is consistent with what was reported by Matrosov et al. (2001, 2012), who measured SLDR, which is practically equivalent to CDR for axisymmetric particles predominantly oriented with their major dimensions in the horizontal plane.

Similar to Z_{DR}, DR tends to decrease in rimed snow relative to aggregated snow. Vogel et al. (2015), Ryzhkov et al. (2016), Kumjian et al. (2016), and Giangrande et al. (2016) claim that Z_{DR} of rimed snow is slightly lower than Z_{DR} of aggregated snow, but this difference is really small (typically 0.2–0.4 dB), which can be clearly visible in the QVP profiles. The corresponding difference in DR is significantly larger (at least 2–4 dB) as can be seen in Fig. 13. Both Z_{DR} and DR exhibit their lowest values in rimed snow just above the melting layer, which is apparently "sagging" during intense riming periods between 1530 and 1630 UTC and between 2100 and 2300 UTC [see also Kumjian et al. (2016) and Xie et al. (2016)]. It is likely that the relative differences of DR between various types of snow/ice may not be much affected by the uncertainty in $\Phi_{DP}^{(t)}$, at least in a qualitative sense. We showed that these differences are maximized if the radar transmits the wave with truly circular polarization, which motivates the utilization of a phase shifter for controlling $\Phi_{DP}^{(t)}$. This, however, does not prevent any dual-polarization radar with simultaneous transmission/reception and arbitrary $\Phi_{DP}^{(t)}$ to use DR for snow classification.

Similar computations of DR from the quasi-vertical profiles of Z_{DR} and ρ_{hv} using Eq. (6) have been made for a number of storms observed with the EEC X-band radar owned by the University of Bonn, Germany (e.g., Diederich et al. 2015). Typical results are illustrated in Fig. 14. Again, the patterns of DR in its QVP profiles at X band are qualitatively and quantitatively similar to the ones obtained from the WSR-88D measurements although the polarization state of the wave transmitted by the X-band radar is not known. The advantage of using DR instead of Z_{DR} for discrimination between rimed and aggregated snow is clearly shown in Fig. 14. Indeed, DR exhibits large differences in snow between the first 30 volume scans (green shades of DR) and the subsequent 40 scans (mainly blue shades of DR). This means that snow was likely more rimed during the later period of observations, which implies a higher supercooled liquid water content favoring more extensive riming of snow.

6. Conclusions

A new methodology for estimating depolarization ratio by dual-polarization radars with simultaneous transmission/reception along with the traditionally measured Z_{DR}, ρ_{hv}, and Φ_{DP} in a single mode of operation has been suggested. This depolarization ratio can serve as a proxy for circular depolarization ratio measured by radars with circular polarization. The suggested methodology implies the use of a high-power phase shifter to control the system differential phase on transmission and a special signal processing to eliminate the detrimental impact of propagation differential phase on the estimate of DR. In the past, the bias related to the differential phase on propagation was a principal obstacle to the use of the directly measured

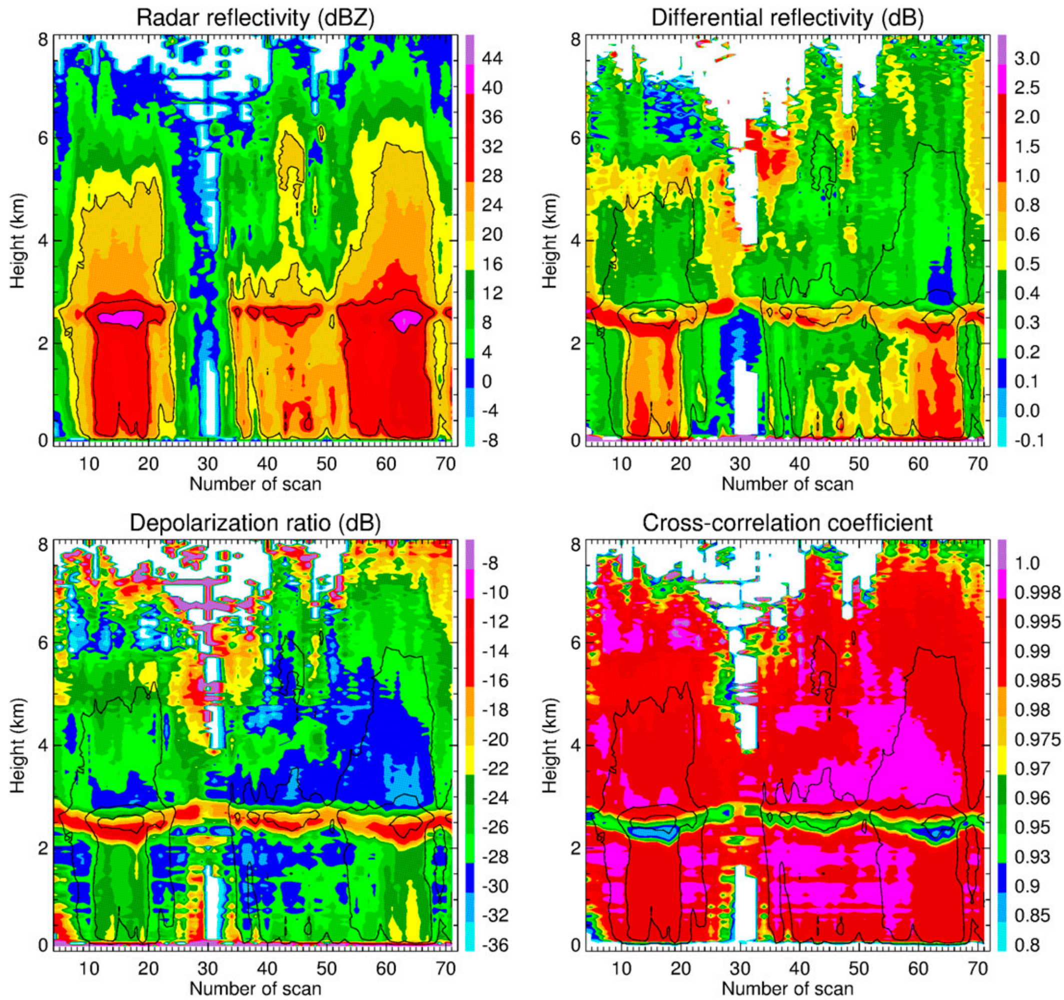

FIG. 14. Composite QVP of Z, Z_{DR}, ρ_{hv}, and DR [estimated from Eq. (6)] obtained from X-band University of Bonn radar at elevation 28.0° on 26 Aug 2014. Radar volume scans are updated every 5 min. Overlaid are contours of Z.

CDR and its earlier estimates from SHV mode measurements (Matrosov 2004). An important advantage of DR (i.e., a CDR proxy) suggested here is also that they are available in the same regions of the radar echo where Z, Z_{DR}, ρ_{hv}, and Φ_{DP} are measured, whereas true CDR measurements can be reliably made only in the areas where the signal-to-noise ratio is significant (i.e., >30 dB) since the echo power in the ''weak'' polarization channel is significantly smaller than the one in the ''strong'' polarization channel.

The feasibility of the recommended approach has been demonstrated by retrieving DR from other polarimetric variables, the raw I–Q data, as well as by implementing the scheme on a C-band radar with simultaneous transmission/reception of the horizontally and vertically polarized waves. It is also shown that the proxy of DR (or CDR) can be roughly estimated from the combination of Z_{DR} and ρ_{hv} measured by radars with arbitrary polarization of the transmitted wave. As opposed to linear depolarization ratio (LDR) (which requires a special mode of operation), DR depends on hydrometeor orientation rather weakly and is less affected by noise.

The suggested approach for estimating depolarization ratios can be implemented with operational weather radars (e.g., the WSR-88D network) and numerous research radars, for example, cloud and precipitation radars operated by the U.S. Department of Energy's Atmospheric Radiation Measurement (DOE ARM) program. The addition of depolarization ratio estimates will improve the utility of the radar measurements to infer microphysical information.

Among potential applications, three major challenging practical tasks can be addressed using DR measurements: 1) detection of hail and determination of its size above the melting layer, 2) discrimination between various habits of ice aloft, and 3) identification and quantification of riming processes associated with the presence of supercooled cloud water and possible icing hazard to aviation.

It is demonstrated that strong convective updrafts where large hail is growing can possibly be better identified as DR columns encompassing most of the updraft as opposed to Z_{DR} columns indicative only of its bottom part. The DR columns are taller because they combine Z_{DR} column and "LDR cap" or ρ_{hv} reduction in a single feature, which can be better detected at higher antenna elevations.

The depolarization ratio proxy estimates can potentially be utilized for the discrimination between different snow types similar to directly measured depolarization ratios. These ratios seem to be noticeably lower in rimed snow than in aggregated snow, and there is a possibility for utilizing DR for the detection of supercooled cloud water, which is an essential ingredient for snow riming.

Meaningful DR values can be estimated from the combination of Z_{DR} and ρ_{hv} measured by polarimetric radars with arbitrary polarization of the transmitted wave for which the differential phase upon transmission $\Phi_{DP}^{(t)}$ is not controlled. It is likely that relative differences of DR between various types of snow/ice may not be much affected by the uncertainty in $\Phi_{DP}^{(t)}$, at least in a qualitative sense. We assume that these differences are maximized if the radar transmits the wave with truly circular polarization, which suggests the utilization of a phase shifter for controlling $\Phi_{DP}^{(t)}$ but does not prevent any dual-polarization radar with simultaneous transmission/reception and arbitrary $\Phi_{DP}^{(t)}$ to use DR for classification of snow.

Acknowledgments. Funding for some of the authors was provided by NOAA/Office of Oceanic and Atmospheric Research under NOAA–University of Oklahoma Cooperative Agreement NA11OAR4320072, U.S. Department of Commerce. Sergey Matrosov was sponsored in part by the U.S. Department of Energy Atmospheric System Research Program under award number DE-SC0013306. Research based on the Bonn X-band radar was carried out in the framework of the Hans-Ertel-Centre for Weather Research (http://www.herz-tb1.uni-bonn.de/) funded by the BMVBS (Federal Ministry of Transport, Building and Urban Development) and the SFB/TR 32 (Transregional Collaborative Research Centre 32, http://www.tr32.de/) funded by the DFG (German Research Foundation).

REFERENCES

Al-Jumily, K., R. Charlton, and R. Humphries, 1991: Identification of rain and hail with circular polarization radar. *J. Appl. Meteor.*, **30**, 1075–1087, doi:10.1175/1520-0450(1991)030<1075:IORAHW>2.0.CO;2.

Aydin, K., and Y. Zhao, 1990: A computational study of polarimetric radar observables in hail. *IEEE Trans. Geosci. Remote Sens.*, **28**, 412–422, doi:10.1109/TGRS.1990.572906.

Barge, B., 1974: Polarization measurements of precipitation backscatter in Alberta. *J. Rech. Atmos.*, **8**, 163–173.

Bringi, V., and V. Chandrasekar, 2001: *Polarimetric Doppler Weather Radar: Principles and Applications.* Cambridge University Press, 636 pp.

——, J. Vivekanandan, and J. Tuttle, 1986: Multiparameter radar measurements in Colorado convective storms. Part II: Hail detection studies. *J. Atmos. Sci.*, **43**, 2564–2577, doi:10.1175/1520-0469(1986)043<2564:MRMICC>2.0.CO;2.

——, K. Knupp, A. Detwiler, L. Liu, L. Caylor, and R. Black, 1997: Evolution of a Florida thunderstorm during the Convection and Precipitation/Electrification Experiment: The case of 9 August 1991. *Mon. Wea. Rev.*, **125**, 2131–2160, doi:10.1175/1520-0493(1997)125<2131:EOAFTD>2.0.CO;2.

Brunkow, D., V. Bringi, P. Kennedy, S. Rutledge, V. Chandrasekar, E. Mueller, and R. Bowie, 2000: A description of the CSU–CHILL National Radar Facility. *J. Atmos. Oceanic Technol.*, **17**, 1596–1608, doi:10.1175/1520-0426(2000)017<1596:ADOTCC>2.0.CO;2.

Carey, L., and S. Rutledge, 1998: Electrical and multiparameter radar observations of a severe hailstorm. *J. Geophys. Res.*, **103**, 13 979–14 000, doi:10.1029/97JD02626.

Chandrasekar, V., and N. Bharadwaj, 2009: Orthogonal channel coding for simultaneous co- and cross-polarization measurements. *J. Atmos. Oceanic Technol.*, **26**, 45–56, doi:10.1175/2008JTECHA1101.1.

Diederich, M., A. Ryzhkov, C. Simmer, P. Zhang, and S. Trömel, 2015: Use of specific attenuation for rainfall measurement at X-band radar wavelengths. Part I: Radar calibration and partial beam blockage estimation. *J. Hydrometeor.*, **16**, 487–502, doi:10.1175/JHM-D-14-0066.1.

Doviak, R. J., and D. Zrnić, 1993: *Doppler Radar and Weather Observations.* 2nd ed. Dover Publications, Inc., 562 pp.

——, V. Bringi, A. V. Ryzhkov, A. Zahrai, and D. S. Zrnić, 2000: Considerations for polarimetric upgrades to operational WSR-88D radars. *J. Atmos. Oceanic Technol.*, **17**, 257–278, doi:10.1175/1520-0426(2000)017<0257:CFPUTO>2.0.CO;2.

Giangrande, S. E., T. Toto, A. Bansemer, M. R. Kumjian, S. Mishra, and A. V. Ryzhkov, 2016: Insights into riming and aggregation processes as revealed by aircraft, radar, and disdrometer observations for a 27 April 2011 widespread precipitation event. *J. Geophys. Res. Atmos.*, **121**, 5846–5863, doi:10.1002/2015JD024537.

Holler, H., V. Bringi, J. Hubbert, M. Hagen, and P. Meischner, 1994: Life cycle and precipitation formation in a hybrid-type hailstorm revealed by polarimetric and Doppler radar measurements. *J. Atmos. Sci.*, **51**, 2500–2522, doi:10.1175/1520-0469(1994)051<2500:LCAPFI>2.0.CO;2.

Holt, A. R., V. N. Bringi, and D. Brunkow, 1999: A comparison between parameters obtained with the CSU-CHILL radar from simultaneous and switched transmission of vertical and horizontal polarisation. Preprints, *29th Int. Conf. on Radar Meteorology*, Montreal, QC, Canada, 214–217.

Huang, G.-J., V. N. Bringi, and M. Thurai, 2008: Orientation angle distributions of drops after an 80-m fall using a 2D-video disdrometer. *J. Atmos. Oceanic Technol.*, **25**, 1717–1723, doi:10.1175/2008JTECHA1075.1.

Hubbert, J. C., and V. N. Bringi, 2003: Studies of the polarimetric covariance matrix. Part II: Modeling and polarization errors. *J. Atmos. Oceanic Technol.*, **20**, 1011–1022, doi:10.1175/1456.1.

——, ——, L. D. Carey, and S. Bolen, 1998: CSU-CHILL polarimetric radar measurements in a severe hailstorm in eastern Colorado. *J. Appl. Meteor.*, **37**, 749–775, doi:10.1175/1520-0450(1998)037<0749:CCPRMF>2.0.CO;2.

——, S. M. Ellis, M. Dixon, and G. Meymaris, 2010: Modeling, error analysis, and evaluation of dual-polarization variables obtained from simultaneous horizontal and vertical polarization transmit radar. Part I: Modeling and antenna errors. *J. Atmos. Oceanic Technol.*, **27**, 1583–1598, doi:10.1175/2010JTECHA1336.1.

Jameson, A., 1987: Relations among linear and circular polarization parameters measured in canted hydrometeors. *J. Atmos. Oceanic Technol.*, **4**, 634–645, doi:10.1175/1520-0426(1987)004<0634:RALACP>2.0.CO;2.

——, M. Murphy, and E. Krider, 1996: Multiple-parameter radar observations of isolated Florida thunderstorms during the onset of electrification. *J. Appl. Meteor.*, **35**, 343–354, doi:10.1175/1520-0450(1996)035<0343:MPROOI>2.0.CO;2.

Kennedy, P. C., and S. A. Rutledge, 2011: S-band dual-polarization radar observations of winter storms. *J. Appl. Meteor. Climatol.*, **50**, 844–858, doi:10.1175/2010JAMC2558.1.

——, ——, W. A. Petersen, and V. N. Bringi, 2001: Polarimetric radar observations of hail formation. *J. Appl. Meteor.*, **40**, 1347–1366, doi:10.1175/1520-0450(2001)040<1347:PROOHF>2.0.CO;2.

Krehbiel, P., T. Chen, S. McCrary, W. Rison, G. Grey, and M. Brook, 1996: The use of dual-channel circular-polarization radar observations for remotely sensing storm electrification. *Meteor. Atmos. Phys.*, **59**, 65–82, doi:10.1007/BF01032001.

Kropfli, R., B. Bartram, and S. Matrosov, 1990: The upgraded WPL dual-polarization 8-mm wavelength Doppler radar for microphysical and climate research. *Conf. on Cloud Physics*, San Francisco, CA, Amer. Meteor. Soc., 341–345.

Kumjian, M. R., A. Khain, N. Benmoshe, E. Ilotoviz, A. Ryzhkov, and V. Phillips, 2014: The anatomy and physics of Z_{DR} columns: Investigating a polarimetric radar signature with a spectral bin microphysical model. *J. Appl. Meteor. Climatol.*, **53**, 1820–1843, doi:10.1175/JAMC-D-13-0354.1.

——, S. Mishra, S. E. Giangrande, T. Toto, A. V. Ryzhkov, and A. Bansemer, 2016: Polarimetric radar and aircraft observations of saggy bright bands during MC3E. *J. Geophys. Res. Atmos.*, **121**, 3584–3607, doi:10.1002/2015JD024446.

Matrosov, S. Y., 2004: Depolarization estimates from linear H and V measurements with weather radars operating in simultaneous transmission–simultaneous receiving mode. *J. Atmos. Oceanic Technol.*, **21**, 574–583, doi:10.1175/1520-0426(2004)021<0574:DEFLHA>2.0.CO;2.

——, 2015: Evaluations of the spheroidal particle model for describing cloud radar depolarization ratios of ice hydrometeors. *J. Atmos. Oceanic Technol.*, **32**, 865–879, doi:10.1175/JTECH-D-14-00115.1.

——, R. F. Reinking, R. A. Kropfli, B. E. Martner, and B. W. Bartram, 2001: On the use of radar depolarization ratios for estimating shapes of ice hydrometeors in winter clouds. *J. Appl. Meteor.*, **40**, 479–490, doi:10.1175/1520-0450(2001)040<0479:OTUORD>2.0.CO;2.

——, ——, and I. V. Djalalova, 2005: Inferring fall attitudes of pristine dendritic crystals from polarimetric radar data. *J. Atmos. Sci.*, **62**, 241–250, doi:10.1175/JAS-3356.1.

——, G. G. Mace, R. Marchand, M. D. Shupe, A. G. Hallar, and I. B. McCubbin, 2012: Observations of ice crystal habits with a scanning polarimetric W-band radar at slant linear depolarization ratios mode. *J. Atmos. Oceanic Technol.*, **29**, 989–1008, doi:10.1175/JTECH-D-11-00131.1.

McCormick, G., and A. Hendry, 1975: Principles for the radar determination of the polarization properties of precipitation. *Radio Sci.*, **10**, 421–434, doi:10.1029/RS010i004p00421.

——, and ——, 1979: Radar measurement of precipitation-related depolarization in thunderstorms. *IEEE Trans. Geosci. Electron.*, **17**, 142–150, doi:10.1109/TGE.1979.294641.

Melnikov, V., and S. Y. Matrosov, 2013: Estimations of aspect ratios of ice cloud particles with the WSR-88D radar. *36th Conf. on Radar Meteorology*, Breckenridge, CO, Amer. Meteor. Soc., 245. [Available online at https://ams.confex.com/ams/36Radar/webprogram/Paper228291.html.]

Minervin, V., and A. Shupyatsky, 1963: Radar method for determining the phase state of clouds and precipitation (in Russian). *Tr. Tsentr. Aerol. Obs.*, **47**, 63–84.

Mirkovic, D., 2016: *Computational Electromagnetics for Polarimetric Radar Scatterers: An Approach to Polarimetric Variable Modeling of Hydrometeors and Biota.* Lambert Academic Publishing, 272 pp.

Ortega, K. L., J. M. Krause, and A. V. Ryzhkov, 2016: Polarimetric radar characteristics of melting hail. Part III: Validation of the algorithm for hail size discrimination. *J. Appl. Meteor. Climatol.*, **55**, 829–848, doi:10.1175/JAMC-D-15-0203.1.

Ryzhkov, A. V., 2001: Interpretation of polarimetric radar covariance matrix for meteorological scatterers. Theoretical analysis. *J. Atmos. Oceanic Technol.*, **18**, 315–328, doi:10.1175/1520-0426(2001)018<0315:IOPRCM>2.0.CO;2.

——, and D. S. Zrnić, 2007: Depolarization in ice crystals and its effect on radar polarimetric measurements. *J. Atmos. Oceanic Technol.*, **24**, 1256–1267, doi:10.1175/JTECH2034.1.

——, ——, J. C. Hubbert, V. N. Bringi, J. Vivekanandan, and E. A. Brandes, 2002: Polarimetric radar observations and interpretation of co-cross-polar correlation coefficients. *J. Atmos. Oceanic Technol.*, **19**, 340–354, doi:10.1175/1520-0426-19.3.340.

——, M. Pinsky, A. Pokrovsky, and A. Khain, 2011: Polarimetric radar observation operator for a cloud model with spectral microphysics. *J. Appl. Meteor. Climatol.*, **50**, 873–894, doi:10.1175/2010JAMC2363.1.

——, M. Kumjian, S. Ganson, and A. Khain, 2013a: Polarimetric radar characteristics of melting hail. Part I: Theoretical simulations using spectral microphysical modeling. *J. Appl. Meteor. Climatol.*, **52**, 2849–2870, doi:10.1175/JAMC-D-13-073.1.

——, ——, ——, and P. Zhang, 2013b: Polarimetric radar characteristics of melting hail. Part II: Practical implications. *J. Appl. Meteor. Climatol.*, **52**, 2871–2886, doi:10.1175/JAMC-D-13-074.1.

——, P. Zhang, Q. Cao, S. Matrosov, V. Melnikov, and M. Knight, 2014: Measurements of circular depolarization ratio with the radar with simultaneous transmission/reception. Extended abstracts. *Eighth European Conf. on Radar in Meteorology and Hydrology*, Garmisch-Partenkirchen, Germany, ERAD, 11.3.

——, ——, H. Reeves, M. Kumjian, T. Tschallener, C. Simmer, and S. Troemel, 2016: Quasi-vertical profiles—A new way to look at polarimetric radar data. *J. Atmos. Oceanic Technol.*, **33**, 551–562, doi:10.1175/JTECH-D-15-0020.1.

Schuur, T. J., A. V. Ryzhkov, and D. R. Clabo, 2005: Climatological analysis of DSDs in Oklahoma as revealed by 2D-video disdrometer and polarimetric WSR-88D. *32nd Conf. on Radar Meteorology*, Albequerque, NM, Amer. Meteor. Soc., 15R.4. [Available online at https://ams.confex.com/ams/32Rad11Meso/webprogram/Paper95995.html.]

Torlaschi, E., and A. Holt, 1993: Separation of propagation and backscattering effects in rain for circular polarization diversity S-band radars. *J. Atmos. Oceanic Technol.*, **10**, 465–477, doi:10.1175/1520-0426(1993)010<0465:SOPABE>2.0.CO;2.

——, and ——, 1998: A comparison of different polarization schemes for the radar sensing of precipitation. *Radio Sci.*, **33**, 1335–1352, doi:10.1029/98RS00633.

Tragl, K., 1990: Polarimetric radar backscattering from reciprocal random targets. *IEEE Trans. Geosci. Remote Sens.*, **28**, 856–864, doi:10.1109/36.58973.

Trömel, S., M. Kumjian, A. Ryzhkov, and C. Simmer, 2013: Backscatter differential phase—Estimation and variability. *J. Appl. Meteor. Climatol.*, **52**, 2529–2548, doi:10.1175/JAMC-D-13-0124.1.

Vogel, J. M., F. Fabry, and I. Zawadzki, 2015: Attempts to observe polarimetric signatures of riming in stratiform precipitation. *37th Conf. on Radar Meteorology*, Norman, OK, Amer. Meteor. Soc., 6B.6. [Available online at https://ams.confex.com/ams/37RADAR/webprogram/Paper275246.html.]

Wang, Y., and V. Chandrasekar, 2006: Polarization isolation requirements for linear dual-polarization weather radar in simultaneous transmission mode of operation. *IEEE Trans. Geosci. Remote Sens.*, **44**, 2019–2028, doi:10.1109/TGRS.2006.872138.

——, ——, and V. Bringi, 2006: Characterization and evaluation of hybrid polarization observation of precipitation. *J. Atmos. Oceanic Technol.*, **23**, 552–572, doi:10.1175/JTECH1869.1.

Williams, E., and Coauthors, 2015: Measurements of differential reflectivity in snowstorms and warm season stratiform systems. *J. Appl. Meteor. Climatol.*, **54**, 573–595, doi:10.1175/JAMC-D-14-0020.1.

Witt, A., M. Eilts, G. Stumpf, J. Johnson, D. Mitchell, and K. Thomas, 1998: An enhanced hail detection algorithm for the WSR-88D. *Wea. Forecasting*, **13**, 286–303, doi:10.1175/1520-0434(1998)013<0286:AEHDAF>2.0.CO;2.

Xie, X., R. Evaristo, C. Simmer, J. Handwerker, and S. Trömel, 2016: Precipitation and microphysical processes observed by three polarimetric X-band radars during HOPE. *Atmos. Chem. Phys.*, **16**, 7105–7116, doi:10.5194/acp-16-7105-2016.

Zrnić, D. S., 1991: Complete polarimetric and Doppler measurements with a single receiver radar. *J. Atmos. Oceanic Technol.*, **8**, 159–165, doi:10.1175/1520-0426(1991)008<0159:CPADMW>2.0.CO;2.